Self-induced sloshing excited by a horizontally injected plane jet

By SOUICHI SAEKI[1], HARUKI MADARAME[2]
AND KOJI OKAMOTO[2]

[1]Department of Mechanical Engineering, Yamaguchi University, Ube,
Yamaguchi, 755–8611, Japan
[2]Nuclear Engineering Research Laboratory, University of Tokyo, Tokai-mura,
Ibaraki 319-1188, Japan

A self-induced free-surface oscillation termed 'self-induced sloshing' was observed in a rectangular tank with a submerged and horizontally injected water jet. Self-induced sloshing is excited by the flow itself without any external force. Its behaviour was examined by experiment. The dominant frequency was found to be close to the first or second eigenvalue of fluid in a tank. The conditions of sloshing excitation were obtained for four tank geometries. They were called the 'sloshing condition', and defined in terms of inlet velocity and water level. Sloshing conditions were found to be strongly dependent on inlet velocity and tank geometry. A two-dimensional numerical simulation code was developed to simulate self-induced sloshing. The code was based on the boundary-fitted coordinate (BFC) method with height function. The numerical results were qualitatively verified by the experimental results, and were found to correlate well in terms of flow pattern, free-surface shape and sloshing conditions. In this study, sloshing growth was evaluated quantitatively using the simulation results. Oscillation energy supplied for the sloshing motion during a sloshing period (E_{con}) was calculated from simulation results. Sloshing growth was found to be strongly related to the sign and magnitude of E_{con}. The distribution of E_{con} showed that jet flow had a strong correlation with the sloshing growth. It was clarified that sloshing growth was primarily dependent on the spatial phase state of jet fluctuation. A governing parameter of self-induced sloshing, the modified Strouhal number St_s, was proposed on the basis of numerical evaluations of oscillation energy. The value of St_s suggests that one or two large vortices generated by jet fluctuations exist between the inlet and outlet during a sloshing period. When St_s is approximately either 1 (*first stage*) or 2 (*second stage*), self-induced sloshing occurs consistently in all experimental cases. The dependence of sloshing on inlet velocity, water level and tank geometry was revealed using St_s. For several tank geometries, a sloshing mode shift or jet mode (stage) transition was found to occur due to changes in inlet jet velocity. The combination of sloshing mode and jet stage can determine the state of the self-induced sloshing. As a result of this study, we propose a new excitation mechanism of self-induced sloshing, represented by a simple feedback loop closed by sloshing motion and jet fluctuation. The overall physical oscillation mechanism of self-induced sloshing was clarified using this feedback loop.

1. Introduction

1.1. *Background*

In recent years, the interaction between a free surface and a submerged vortical flow in a tank has attracted the attention of nuclear engineers. It is being applied to, for example, the liquid metal fast breeder reactor (LMFBR), where free-surface flow conditions exist in the reactor vessel (Inagaki *et al.* 1987). The vessel was designed to be as small as possible in order to reduce construction costs. As a result, high-speed flow of the sodium coolant was required to remove sufficient heat from the core. Reactor safety design criteria require that free-surface flow remains stable under all operating conditions. High-speed flow under the free surface, however, may cause undesirable surface phenomena, e.g. breaking waves, gas entrainment and self-induced free-surface oscillation.

One surface phenomenon is self-induced sloshing excited by the flow itself. This oscillating phenomenon must be prevented from occurring under any operating condition. Clarification of the excitation mechanism of each free-surface oscillation caused by the interaction between free surface and submerged vortical flow is therefore required.

Several kinds of self-induced free-surface oscillations have been experimentally observed in a tank system with a free surface and a submerged jet, e.g. 'jet-flutter', 'self-induced U-tube oscillation' and 'self-induced sloshing'. Jet flutter is a self-induced oscillation caused by an upward plane jet impinging on a free surface (Madarame *et al.* 1993). This oscillation is accompanied by horizontal fluttering of the surface swell that forms on jet impingement. Self-induced U-tube oscillation is a coupled oscillation of two free surfaces in a U-shaped double-tank system, namely an upstream and downstream tank (Okamoto, Fukaya & Madarame 1993). In this case, two separated surfaces move up and down alternately with a remarkable variation in the flow pattern in the upstream tank. Studies on self-induced sloshing are mentioned briefly in § 1.3.

1.2. *Self-induced sloshing*

Self-induced sloshing was discovered by Okamoto & Madarame (1991), caused by a horizontally injected plane jet in a rectangular tank. Figure 1 shows a schematic view of a test tank. The submerged water jet was injected horizontally into the tank from an inlet on the left-hand wall. At a certain inlet velocity and water level condition, the free surface oscillated periodically in the first or second mode, i.e. 'Self-induced sloshing' (Okamoto & Madarame 1991; Okamoto, Madarame & Fukaya 1993). Similar phenomena were subsequently observed in several different tank geometries (Fukaya *et al.* 1993). Self-induced sloshing is the natural oscillation of fluid in a tank excited by the flow in the absence of other external forces. Sloshing is generally excited under conditions of relatively low inlet velocity and low water level. A certain experimental tank geometry can exhibit the same mode or multi-mode sloshings under two separate inlet velocity conditions. In this study, the excitation mechanism of this phenomenon is evaluated experimentally and numerically.

1.3. *Previous studies on sloshing and self-induced sloshing*

Many experimental, numerical and theoretical studies on sloshing have been conducted (Abramson, Chu & Kana 1966; Hara 1990). Abramson *et al.* (1966) experimentally and theoretically investigated nonlinear characteristics of the amplitude–frequency response of sloshing forced by a lateral excitation in containers of various
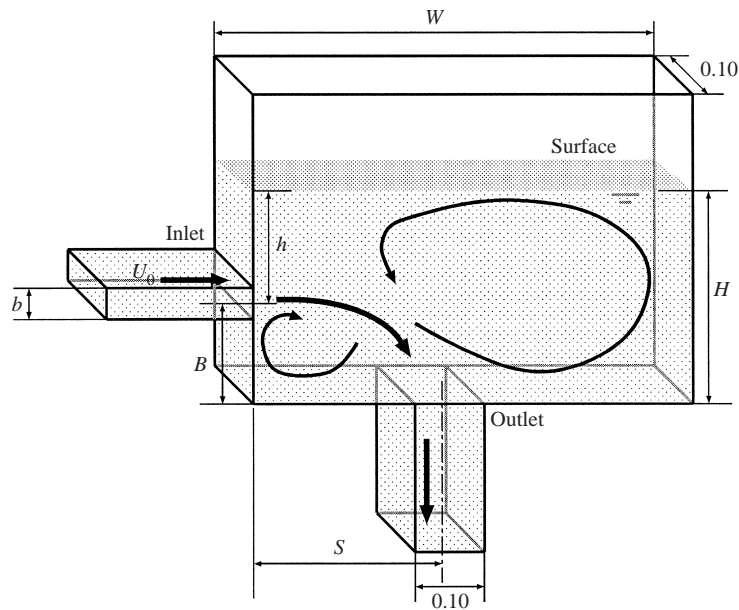
FIGURE 1. Schematic view of the test tank (dimensions in mm).

geometries. Hara (1990) experimentally and theoretically evaluated the frequency response characteristics of forced sloshing under some flow-circulation patterns in a rectangular container. The main objective of these studies was to investigate the nonlinearities of free-surface oscillation induced by an external force with or without a steady flow below the free surface. In contrast, there have been only a few studies on self-induced sloshing in the absence of other external forces.

A few numerical simulations of self-induced sloshing have been performed (Amano & Iwano 1991; Takizawa, Koshizuka & Kondo 1992) and numerical growth models have been proposed using simulation results (Takizawa & Kondo 1995). Amano & Iwano (1991) simulated first mode sloshing using the vortex method, and qualitatively concluded that the phenomenon was excited by an imbalance of the vortices formed over and under the jet near the inlet. Takizawa *et al.* (1992) used the physical components boundary fitted coordinate (PCBFC) method and showed that the free surface oscillated at certain inlet velocity and water level conditions. Based on simulation results, a model was proposed in which sloshing growth was attributed to the flow directly under the free surface containing secondary flow caused by surface potential variation (Takizawa & Kondo 1995). Oscillation energy was assumed to be transferred from the kinetic energy of forced circulation by a nonlinear wave created by the secondary flow. Using Takizawa & Kondo's model, however, it was difficult to analyse the growth mechanism quantitatively.

Several experimental and theoretical models of self-induced sloshing excited by a horizontally injected jet have been proposed (Okamoto & Madarame 1991; Madarame, Okamoto & Hagiwara 1992). It was found experimentally by Okamoto & Madarame (1991) that pattern transformation of circulating flow with free-surface elevation caused first mode sloshing. Oscillation energy was thought to be supplied by surface potential variations due to flow pattern transformation. Madarame *et al.* (1992) proposed a theoretical model of first mode sloshing, which assumed superposition of vortex potential and sloshing potential. Oscillation energy was thought
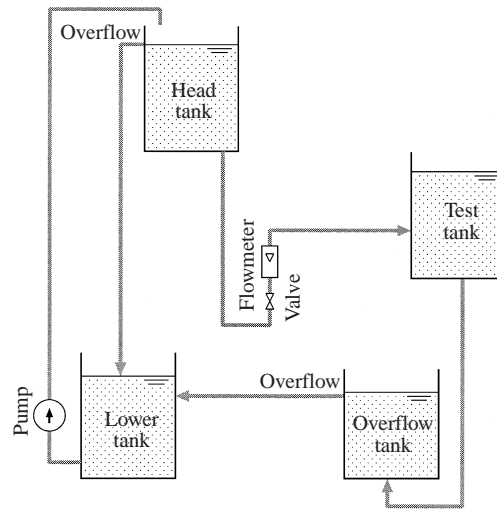
FIGURE 2. Schematic diagram of the test loop.

to be supplied by pressure fluctuations caused by interaction between circulating flow and sloshing motion. All of these models failed to exhaustively explain the dependence of first mode self-induced sloshing on inlet velocity, water level and tank geometry. None of the models have been applied to second mode self-induced sloshing or to the observation of two separate sloshing conditions with respect to inlet velocity. Furthermore, few proposed mechanisms were able to explain sloshing excitation quantitatively, because the complexity of flow with a free surface prevented experimental and theoretical models from revealing the self-induced oscillation system of this phenomenon.

1.4. *Objectives*

The overall objective of the present study is to determine the excitation mechanism of self-induced sloshing excited by a horizontally injected plane jet. The characteristics of this phenomenon are experimentally investigated in §2. However, it proved difficult to evaluate the excitation mechanism using only experimental results, because it was necessary to obtain highly resolved time and space data. In order to obtain detailed complete flow field data, a numerical simulation of self-induced sloshing is conducted and is verified by the experimental results in §3. Simulation results are used quantitatively in the analysis of the sloshing in §4. In §5, based on the results of the numerical analysis, a governing parameter is modified to present the experimental results consistently. A growth mechanism is proposed, based on the physical interpretation of numerical analysis and the modified governing parameter. Furthermore, by comparing with other self-induced flow vibrations, e.g. 'edge tone' and 'edge tone having a resonator' (Blake 1986; Rockwell & Naudascher 1979; Brackenridge & Nyborg 1956), the features and mechanism of self-induced sloshing were evaluated in a consistent manner.

2. Experiment and results

2.1. *Experimental setup and procedure*

In order to examine the dynamics of a free surface with high-speed flow in a tank, a simple two-dimensional rectangular test tank was used. Figure 2 shows the schematic

Tank	b	W	B	S	State	[Mode]
A	**100**	1000	250	500	Sloshing	[1]
C	100	1000	**450**	500	Sloshing	[1]
M	**20**	1000	250	375	Sloshing	[1 or 2]
N	20	1000	**375**	375	Sloshing	[1 or 2]

TABLE 1. Geometric parameter of test tank (unit: mm).

diagram of the flow loop system used with the test tank. Water was pumped up from the lower tank to the head tank, from which the inlet flow was supplied to the test tank. The head tank water level was maintained constant by an overflow system, so as to prevent pump vibration from occurring. The inlet flow rate was valve-controlled and measured by a floating-type flow meter. The cross-section of the overflow tank was constructed to be 10 times larger than that of the test tank. Therefore, the flow rate variation of the overflow tank is estimated to be about 5%, so can be considered negligible. All structures were firmly fixed to the floor, and no resonant fluid oscillation induced by structural vibration was observed.

Figure 1 schematically represents the test tank, where a transparent acrylic board was used as the front wall of the tank for observation. In order to restrict the flow to two dimensions, the thickness of the test tank was constructed to be 100 mm, which was much smaller than the tank width. The test tank had a rectangular inlet on the left-hand sidewall and an outlet on the bottom. The inlet duct length was 600 mm, which was more than 5 times as large as the inlet hydraulic diameter. The inlet jet flow is qualitatively considered to be a developed turbulent jet. The test tank was connected to the overflow tank by the outlet duct, the length of which was 500 mm. The tank geometry could be changed by adding solid inserts. The geometrical parameters are inlet height from the bottom B, outlet location from the inlet sidewall S, inlet width b and tank width W, as shown in figure 1. Table 1 shows the geometries of four representative test tanks: they can be broadly categorized into two groups with inlet width $b = 100$ and 20 mm, respectively. Only parameter B is changed within a tank group. Tank A was defined as the standard experimental test tank.

For each tank geometry, characteristics of the free surface and flow field were observed on varying inlet velocity U_0 and mean water level H. Inlet velocity U_0 was calculated from the inlet flow rate divided by the cross-sectional area of the inlet. Mean water level H was controlled by an overflow-tank gate. The free surface was not completely flat, so water level H was defined as the distance between the free surface and the tank bottom near the inlet sidewall. Water level elevation data were obtained by a condenser-type level meter, which was constructed of a 7 mm diameter glass tube containing a thin copper wire. The water level was calculated from the electric capacity curve of the wire when in water. The free-surface profiles were observed by CCD camera and recorded by VTR. The free-surface shape was measured from digitized surface profiles using image processing.

The unsteady flow pattern was measured using particle image velocimetry (PIV) (Adrian 1991). The oscillating flow was observed to be clearly restricted to two dimensions because the tank thickness was 10 times smaller than the tank width. Therefore, the whole field could be illuminated by halogen lamps above the free surface.

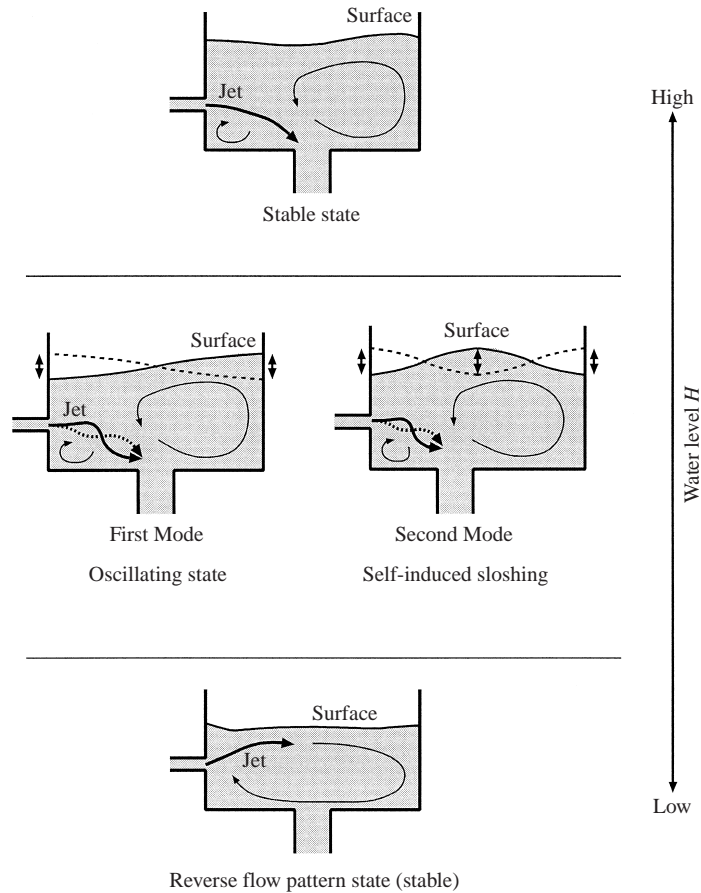The oscillating flow in the tank was visualized by seeding with plastic particle

FIGURE 3. Schemata of flow states.

tracers with a diameter of about 0.8 mm and specific gravity of about 1.02. Since the target flow field was relatively large, these relatively large particles were used. The particle images were captured by a 120 Hz high-speed digital camera. The image resolution was 640×480 with 8 bit intensity depth. The camera could capture about 180 images which were equivalent to about 1.4 s. Thus, this camera system was capable of recording images for a complete sloshing cycle of about 1.2 s. Two-dimensional velocity distributions were calculated from flow images using the simple direct cross-correlation method for PIV. The interrogation area was 32×32 pixels with 50% overlap. There were a lot of erroneous vectors in calculated flow fields due to the halogen lamp illumination etc. Therefore, phase averaging was applied to remove experimental noise. Using an average of 18 cases, the phase-averaged flow field was calculated for every $\pi/24$ cycles, hence 48 flow fields were obtained for one cycle. Phase-averaged velocity data were estimated to contain about 20% erroneous vectors. However, this is sufficiently accurate to evaluate the flow fluctuation qualitatively.

2.2. *Experimental results*

2.2.1. *Flow pattern in the stable state*

The flow state was dependent on test tank geometry, inlet velocity U_0 and water level H. Three states of flow were observed: 'stable', 'oscillating' and 'reverse flow
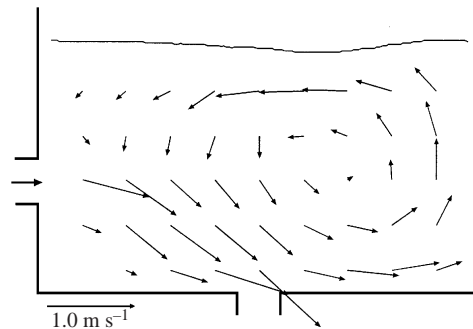
FIGURE 4. Velocity distribution and surface shape of the stable condition (Tank A) under the condition of $U_0 = 1.0 \, \text{m s}^{-1}$ and $H = 0.55 \, \text{m}$.

pattern', as shown by figure 3. Characteristics of the oscillating state are explained in §2.2.2.

Figure 4 shows a typical velocity distribution and free-surface profile. In the stable state, the free surface and the flow pattern were stable and unique. The submerged water jet entered the test tank from the inlet channel, then turned downward to the outlet. An underwater surface stream was observed to flow from the far sidewall toward the inlet sidewall. A large counterclockwise circulating flow was present on the far side of the test section, while a small clockwise circulating flow was observed at the bottom inlet corner below the jet. The small circulation is not shown in figure 4, because the tracer particle density was low in the vicinity of the inlet and outlet. When observing the entire flow field ($W = 1.0 \, \text{m}$), it was difficult to track the scattered light signals from particles around the high-velocity area, e.g. the jet.

When the water level was low and close to the inlet, the reverse flow pattern state was observed, as shown in figure 3. Only one large clockwise circulating flow appeared, and the stream below the free surface flowed in the opposite direction to that of the stable state. Because the turbulent jet was attached directly to the free surface, a rough wavy surface and bubble entrainment were observed. However, a periodic free-surface oscillation (sloshing) could not be excited.

2.2.2. *Self-induced sloshing*

For a certain tank geometry with inlet velocity U_0 and water level H, self-induced free-surface oscillation was observed. Figure 5(a) shows that the oscillation amplitude is reaching 80 mm which is considerably larger than the mean water level $H = 0.63 \, \text{m}$ and tank width $W = 1.0 \, \text{m}$. Variations in inlet flow rate and structural vibrations were not observed even in the oscillation state. This free-surface oscillation is 'self-induced sloshing', which is excited by the flow itself without any external force. In contrast, figure 5(b) shows the stable state, where the oscillation amplitude is lower and diminishing with time.

Figures 6(a) and 6(b) show two examples of free-surface shape variations over a sloshing period. Figure 6(a) shows first mode self-induced sloshing, where the both ends of the surface move up and down alternately with a node at the centre. A nonlinear wave was seen superposed on the standing wave. It was generated synchronously with the sloshing motion, and propagated against the free-surface flow. Figure 6(b) shows second mode self-induced sloshing, where the both ends of the surface oscillate in the same phase with two nodes. The phase difference between the ends and the midpoint of the surface is 180°.
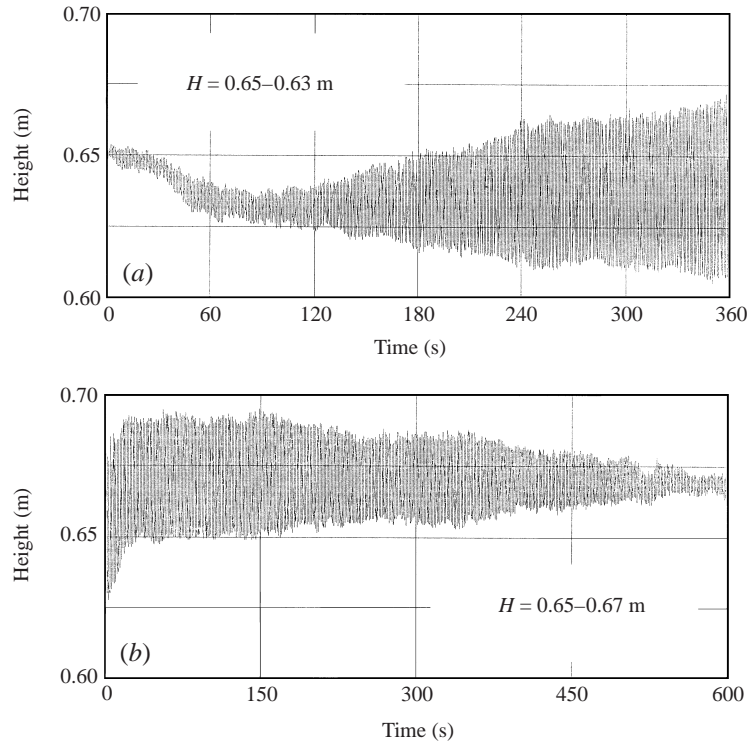
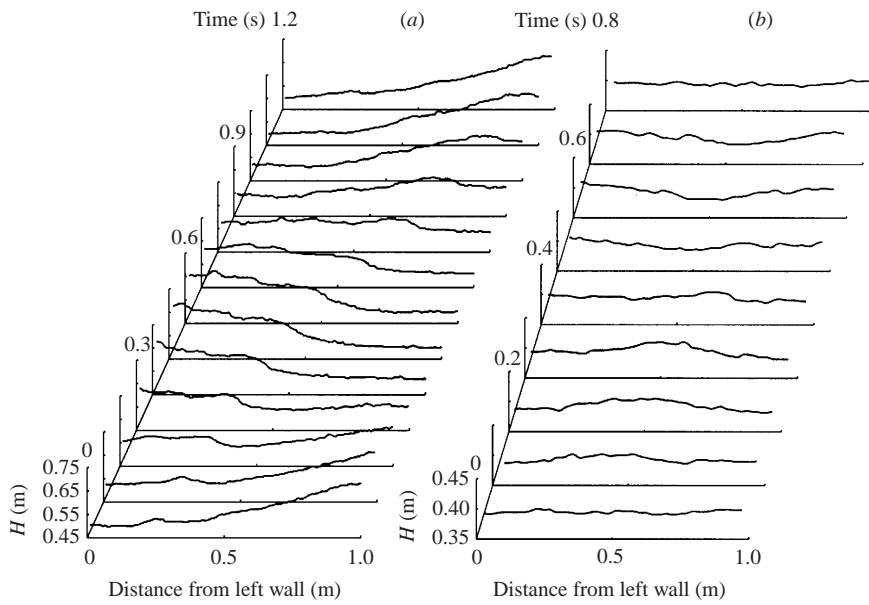FIGURE 5. Free surface oscillation (Tank A); $U_0 = 0.67\,\mathrm{m\,s^{-1}}$.

FIGURE 6. Free surface shape: (*a*) first mode sloshing (Tank A) $U_0 = 0.75\,\mathrm{m\,s^{-1}}$, $H = 0.55\,\mathrm{m}$, and (*b*) second mode sloshing (Tank M) $U_0 = 0.75\,\mathrm{m\,s^{-1}}$, $h = 0.55\,\mathrm{m}$.

Jet oscillation was found only at the sloshing condition, and was the most remarkable behaviour in the unsteady flow pattern. Hence, self-induced sloshing was excited only when one circulation was present on each side of the jet, as shown in figure 3. It was observed using blue dye that the jet oscillated at an asymmetric mode when synchronized with sloshing motion. Detailed features of jet oscillation are examined using PIV in §2.2.7.

2.2.3. *Oscillation frequency*

Figures 7(*a*) and 7(*b*) show examples of the dominant frequencies with respect to water level H under the sloshing condition. The dominant frequencies were obtained from time-series water level data, using the fast fourier transform (FFT). Resolution of the frequencies obtained was better than 0.005 Hz. The theoretical frequency of nth mode sloshing without circulating flow is given by (Lamb 1932).

$$f_s^n = \frac{1}{2\pi} \sqrt{g\frac{n\pi}{W} \tanh\left(\frac{n\pi}{W}H\right)}, \tag{2.1}$$

where the superscript n denotes the mode of sloshing and g is gravitational acceleration. The theoretical frequencies (2.1) are represented by lines in figure 7, and can be seen to increase monotonically with increasing water level. Experimental frequencies were in good agreement with the theoretical prediction.

2.2.4. *Experimental excitation map*

Figure 8 shows excitation maps for each geometrical test tank case with respect to inlet velocity U_0 and inlet–surface distance $h = H - B$. In the experiment, the sloshing condition was defined to occur when the amplitude of the free-surface oscillation after 120 s exceeded 0.01 m.

Each excitation map is quite different in spite of only small changes in tank geometry. Thus, the sloshing condition depends strongly on tank geometry. In all tank cases, the sloshing condition was restricted to certain regions of U_0 and h. The excitation of self-induced sloshing was observed overall to have maximal and minimal limits of U_0 and h for a given tank geometry. For example, the sloshing condition with respect to U_0 was from 0.3 to 1.5 m s^{-1} in all cases. The minimum and maximum of U_0 are considered to be determined by inlet energy and supercritical flow below the free surface. The maximal limit of inlet–surface distance h was about 0.5 m. The free surface and the flow tended to be stable with increasing h. Under higher water level conditions, more energy is required to induce free-surface oscillation. The minimal limit $h = 0.1$ m was determined by the transition of the flow pattern. When the inlet–surface distance was shorter, the jet was directed toward the surface, resulting in the reverse flow pattern. Self-induced sloshing was not observed in this flow pattern.

Tank A, Tank M and Tank N had two separate sloshing regions of the same or a different mode of oscillation. In the case of Tank A, self-induced sloshing occurred under two separate conditions: high velocity *first stage sloshing* and low velocity *second stage sloshing*. Both were dominated by first mode sloshing. Under inlet velocity conditions between those of first and second stage sloshing, self-induced sloshing did not occur at all. Therefore, sloshing growth is considered to be strongly dependent on inlet velocity. In the cases of Tank M and Tank N, first and second mode self-induced sloshing conditions were distributed differently as shown in figures 8(*c*) and 8(*d*). Sloshing in the first mode was observed in Tank M at higher inlet velocities and in the second mode at lower velocities. On the other hand, Tank N exhibited first mode sloshing at lower inlet velocities and second mode sloshing at higher velocities.
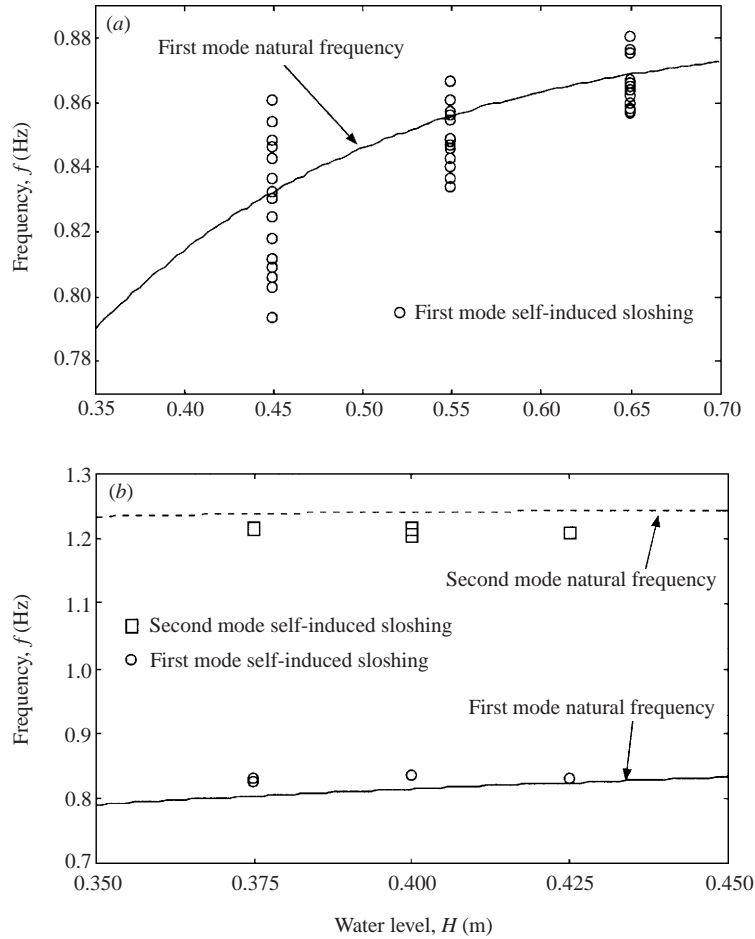
FIGURE 7. Frequency of self-induced sloshing: (*a*) first mode sloshing (Tank A), and (*b*) second mode sloshing (Tank M).

The occurrence of multi-mode sloshing is strongly dependent on both inlet velocity and tank geometry, as can be seen from table 1 where small change in S for Tank M and Tank N appears to invoke multi-mode sloshing. Furthermore, second mode sloshing was not observed in a tank having a large inlet nozzle width ($b = 100\,\text{mm}$), e.g. Tank A. The occurrence of the multi-mode sloshing is regarded as also determined by the inlet nozzle width b.

Consequently, self-induced sloshing was found to be very sensitive to inlet velocity and tank geometry. To further investigate the phenomenon, physical parameter dependences on inlet velocity, e.g. growth ratio, frequency and flow pattern, are examined in the standard case of Tank A in following sections.

2.2.5. *Growth ratio*

The growth rate γ of the free-surface oscillation was calculated from the amplitude variation of the free surface A_i, based on the linear theory: $\gamma = \ln(A_{i+1}/A_i)$. Subscript i denotes the arbitrary step number of free-surface oscillation. The normalized growth ratio $G = \gamma/|\gamma_0|$ is defined as the growth rate γ divided by the absolute value of growth
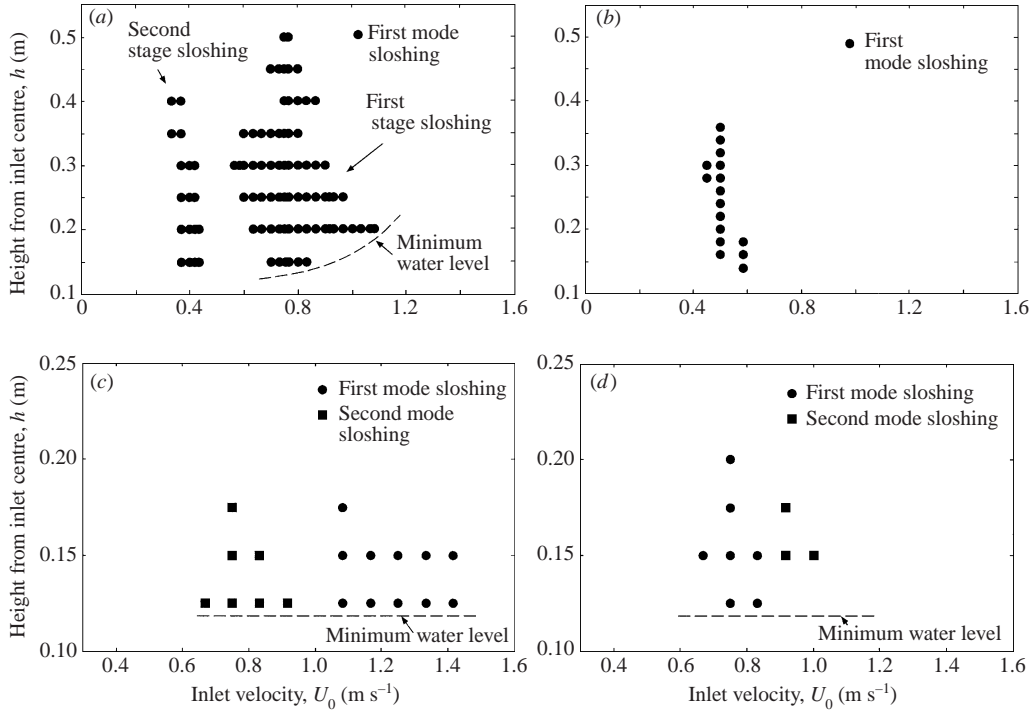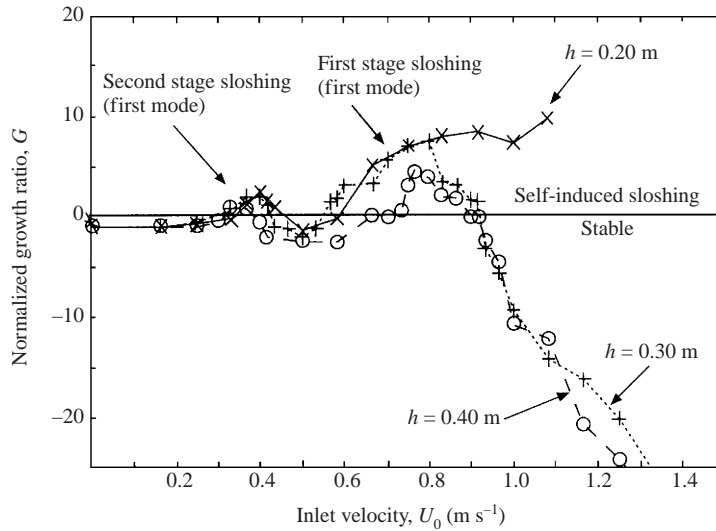
FIGURE 8. Excitation map: (*a*) Tank A, (*b*) Tank C, (*c*) Tank M, (*d*) Tank N.

FIGURE 9. Relationship between U_0 and growth ratio G.

rate γ_0 without inlet flow ($U_0 = 0$). When the free-surface oscillation is self-excited or damped, G is positive or negative, respectively.

Figure 9 shows the normalized growth ratio G in Tank A against inlet velocity U_0. With increasing U_0, G tended to decrease rapidly, resulting in the stable condition ($G < 0$). With increasing inlet–surface distance h, G also tended to shift toward negative values. In the region between first and second stage sloshing, self-induced
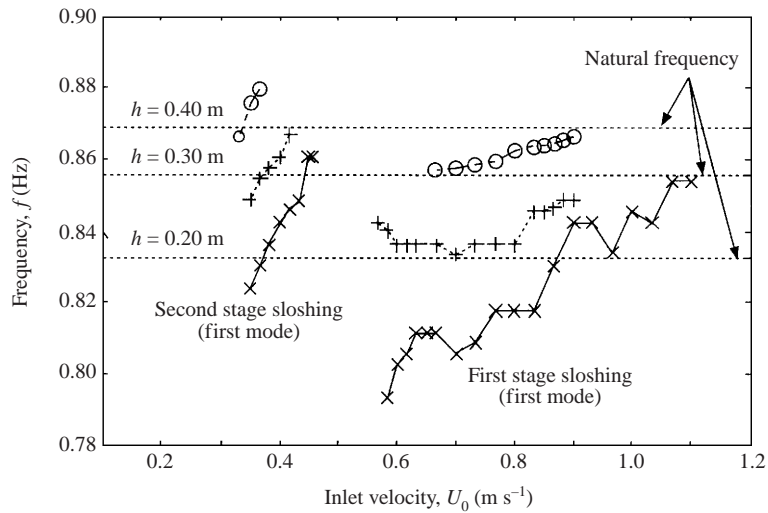
FIGURE 10. Relationship between U_0 and frequency f.

sloshing was not observed because G was negative. Hara (1990) reported that the damping rate of sloshing motion increased rapidly with increasing flow velocity under the free surface. The present result is very similar to Hara's experimental result. The flow velocity under the free surface is assumed to be nearly proportional to inlet velocity U_0, and so the excitation of self-induced sloshing is considered to be restricted by a corresponding rise in damping. From the analysis of growth ratio, therefore, it is suggested that limitation of sloshing conditions could be dependent on the flow velocity under the free surface.

2.2.6. *Relationship between frequency and inlet velocity*

Figure 10 shows dominant frequencies against inlet velocity U_0. The dashed lines represent the theoretical eigenvalues obtained from (2.1) with respect to inlet–surface distance $h = H - B$. Experimental frequencies were close to the theoretical prediction; however they were found to increase by about 7% with increasing inlet velocity. In particular, this tendency was strong under the lower water level and inlet velocity conditions. The dominant frequency of self-induced sloshing is considered to be dependent on inlet velocity U_0.

Hara (1990) examined the frequency response of sloshing excited by a lateral force by varying the averaged under-surface flow velocity. Sloshing frequencies were experimentally and theoretically proven to decrease with increasing the under-surface flow velocity. The dominant frequencies of self-induced sloshing under the higher velocity condition are on average lower than theoretical eigenvalues. However, the tendency for the dominant frequency of self-induced sloshing to increase is quite different from the results of Hara. Hence, this tendency is considered to be a characteristic of self-induced sloshing, and to originate in the sloshing growth mechanism.

2.2.7. *Velocity distribution of fluctuating jet flow*

The turbulent jet flow from inlet to outlet was analysed primarily using particle image velocimetry (PIV) because the test tank was relatively large and jet fluctuation was the most remarkable phenomenon under consideration. Inlet–surface distance h and tank geometry were fixed at $h = 0.20$ m and Tank A, respectively. PIV was
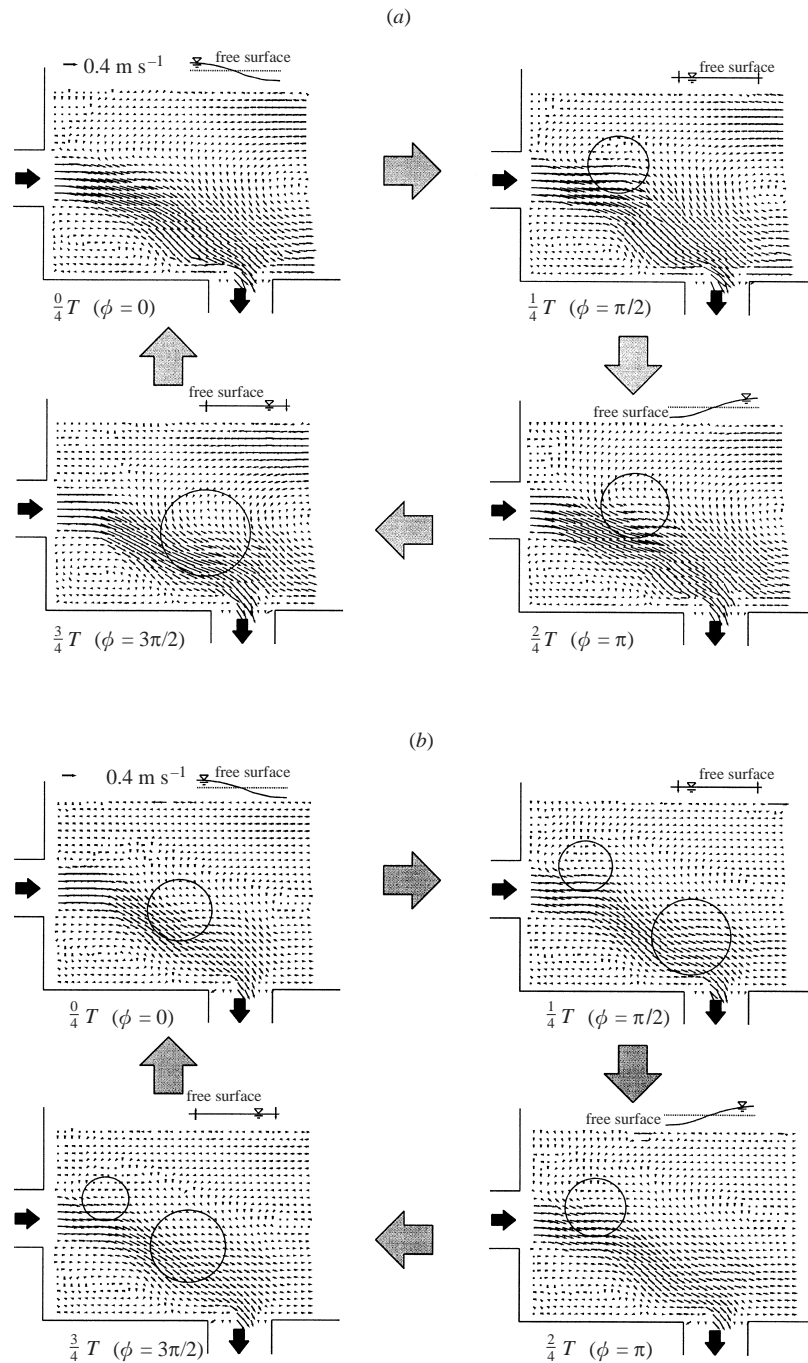
(a)

(b)

FIGURE 11. Velocity distribution: (a) first stage sloshing; (b) second stage sloshing ($U_0 = 0.60 \, \text{m s}^{-1}$, $h = 0.20 \, \text{m}$).

conducted under two separate sloshing conditions, $U_0 = 0.6 \, \text{m s}^{-1}$ (first stage sloshing) and $U_0 = 0.3 \, \text{m s}^{-1}$ (second stage sloshing), since the sloshing stages were strongly related to inlet velocity.

Figures 11(a) and 11(b) show jet fluctuation over a sloshing period, for first
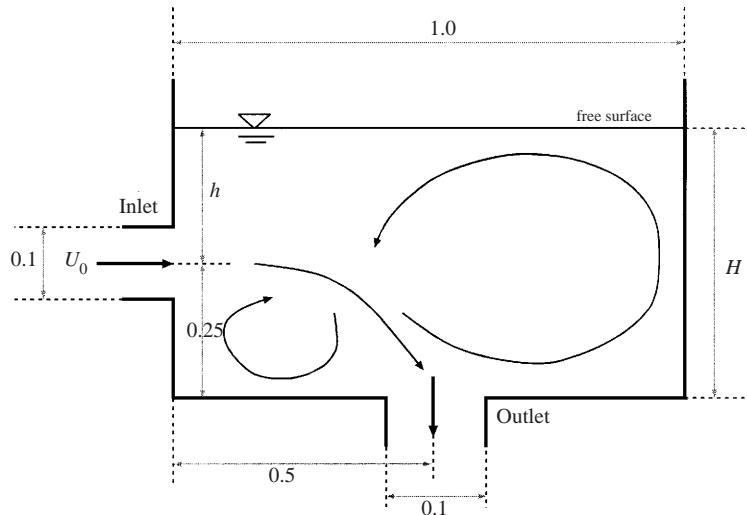
FIGURE 12. Test tank for numerical simulation (Tank A) (dimensions in m).

and second stage sloshing, respectively. The representative velocity of the jet was observed to be approximately the averaged inlet velocity U_0, so the inlet jet flow was qualitatively confirmed to be a developed turbulent jet. The jet was found to oscillate asymmetrically and wavily, and to be synchronized with the sloshing motion. The wave number of the jet fluctuation for second stage sloshing was observed to be nearly twice that for first stage sloshing. As shown in figure 11, jet fluctuation caused one or two large vortices to form and be transported along the jet toward the outlet. For first and second stage sloshing, respectively one and two large vortices caused by sloshing motion could be seen from inlet to outlet at any instant in time. Therefore, the mode, i.e. the spatial phase of jet fluctuation, is considered to be quite different under the two conditions. It was qualitatively proven that the mode of jet fluctuation affected the excitation.

3. Numerical simulation and verification

3.1. *Numerical simulation code*

A two-dimensional laminar code was developed to simulate self-induced sloshing. This code numerically simulated transient flow with a free surface in a rectangular tank with a horizontally injected plane jet. Figure 12 schematically depicts the simulated test tank. Although the actual flow has three-dimensionality, self-induced sloshing can be assumed to be two-dimensional in the case of a thin rectangular tank. In the experiment, the turbulence of the inlet jet has a Reynolds number of more than 10^4. However, the turbulent boundary condition at the free surface is unknown. Takizawa *et al.* (1992) reported that self-induced sloshing could be simulated by a laminar code. In order to extract and simplify the main characteristics of this phenomenon, two-dimensional laminar flow was assumed in this simulation.

3.1.1. *Numerical simulation technique*

A simulation of flow with a free surface is difficult because of the moving boundary condition at the free surface. Many numerical simulation methods have been proposed to predict flow with a free surface, e.g. the VOF method (Nichols, Hirt & Hotchkiss

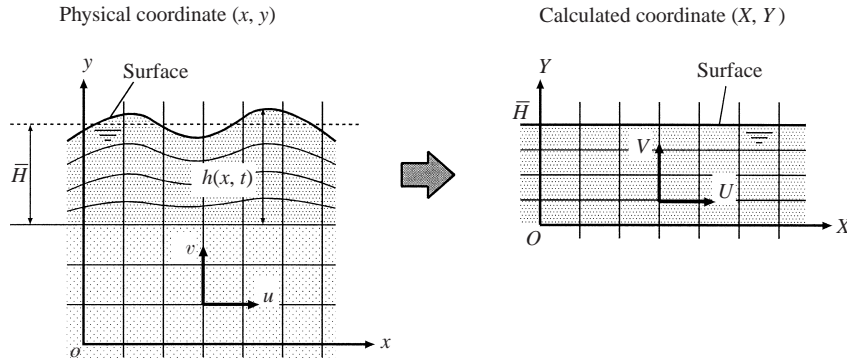Physical coordinate (x, y) Calculated coordinate (X, Y)

FIGURE 13. Transformation in BFC method applied with height function $h(x, t)$.

1980). In this study, the boundary fitted coordinate (BFC) method was applied with the height function method (Tanaka & Fukuhara 1996). This method reproduces flow with a free surface by the algebraic method of coordinate transformation. The shape of the free surface $h(x, t)$ is defined by a single-valued function of one coordinate axis, i.e. the horizontal coordinate axis x in figure 13. An axis η introduced in the BFC method is obtained by the normalization of the vertical coordinate axis y by $h(x, t)$. The shape of the free surface $h(x, t)$ in the physical coordinate system (x, y) can be transformed to the constant water level H in the coordinate system (X, Y) using the following coordinate transformation

$$X = x, \quad Y = \eta H = (y/h(x, t))H. \tag{3.1}$$

The Navier–Stokes and continuity equations were solved using staggered grids in this rectangular calculation coordinate system (X, Y). The coordinate transformation was applied only to the flow near the free surface (BFC region). In the other region (the normal coordinate region), a normal Cartesian coordinate system was used in order to reduce calculation time. The regions were connected using cubic interpolation. This simulation code is based on the FDM (finite difference method) and SIMPLE method (semi implicit method for pressure linked equations). In the Navier–Stokes equation, unsteady terms and diffusion terms were discretized using Crank–Nicholson and centred differences methods, respectively. Convection terms were discretized using third-order upwind differences, i.e. the Kawamura & Kuwahara (1984) scheme.

3.1.2. *Boundary conditions and other conditions*

Duct nozzles were connected to the test tank at the inlet and outlet. Inlet velocity was fixed at $u = U_0$. The pressure gradient at the inlet and outlet was zero, $\partial p/\partial x|_{inlet} = 0$ and $\partial p/\partial y|_{inlet} = 0$, respectively. The outlet boundary condition was defined such that the velocity gradient in the vertical direction was zero, $\partial v/\partial y|_{outlet} = 0$. Thus, the flow rate at the outlet was equivalent to that at the inlet.

The boundary condition at the wall was defined to be free-slip. A constant gas pressure $P_{atm} = 0$ was defined to balance at the free surface with the fluid pressure gradient and surface tension in the normal direction, assuming that the tangential stress at the free surface is negligible. The contact condition between the free surface and the wall was defined to be free-slip.
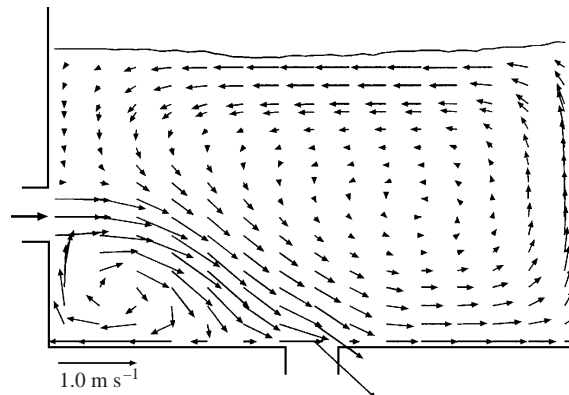
FIGURE 14. Simulated flow pattern and surface shape of the stable condition (Tank A) for $U_0 = 0.8\,\mathrm{m\,s^{-1}}$ and $H = 0.55\,\mathrm{m}$.

In the simulation, the Reynolds number Re and Weber number We were fixed at 500 and 5.0, respectively, defined with respect to inlet velocity U_0 and inlet jet nozzle width b. Therefore, when U_0 is varied, kinematic viscosity v and surface tension σ also vary, and are much larger than the conditions in the experiment. The time step Δt was not more than 2.0×10^{-3} s. The mesh size $\Delta x \times \Delta y$ was approximately $0.01\,\mathrm{m} \times 0.01\,\mathrm{m}$ and the total number of grit points was about 4000. Halving Δt and $\Delta x \times \Delta y$ had little effect on the simulation results. The simulation began by proportionally increasing inlet velocity U_0 and drain velocity from zero for about 10 s.

The simulated test tank as shown in figure 12 is a two-dimensional representation of the standard experimental tank, i.e. Tank A. The simulation was carried out for this tank with varying inlet velocity U_0 and water level H, which was similar to the experimental procedure. At a certain condition, free-surface oscillation was observed, i.e. numerical self-induced sloshing. The occurrence of numerical self-induced sloshing was defined in the same way as in the experiment.

3.2. *Verification of simulation results*

In order to evaluate sloshing growth by means of numerical simulation, it is necessary to validate the simulation results. It is clear that the two sets of experimental and numerical results will not agree quantitatively because of some assumptions in the simulation. For instance, three-dimensionality and turbulence were not considered in this simulation. However, if the excitation mechanism of numerical self-induced sloshing can be identified as the same as that in the experiment, then it is considered possible to use the simulation to analyse the mechanism. Therefore, the simulation results do not have to be quantitatively compared with the experimental results, i.e. for the same condition of inlet velocity U_0 and water level H. Verifications of the present numerical simulation are conducted qualitatively as follows.

3.2.1. *Simulated flow pattern in the stable state*

Figure 14 shows a simulated flow pattern in a stable condition. It was qualitatively consistent with the experiment shown in figure 4. This code is therefore generally considered to simulate flow with a free surface correctly, except for conditions of very low water level and high speed flow. Flow under these exceptional conditions could not be simulated, because the free surface diverged numerically due to the large
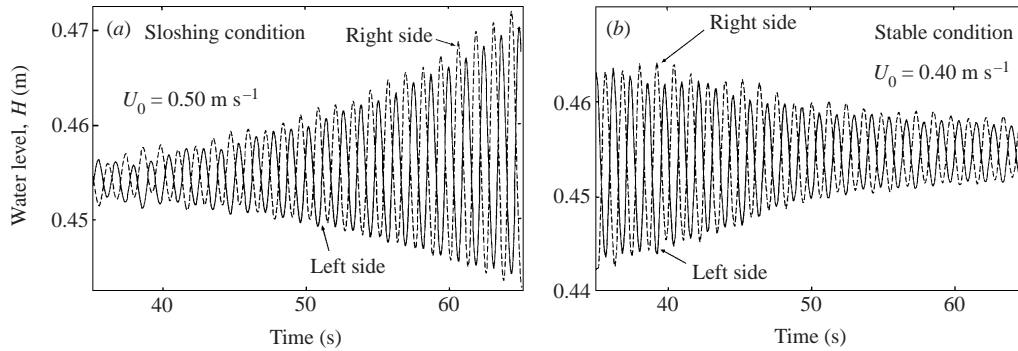
FIGURE 15. Simulated free-surface oscillation for $H = 0.45$ m.
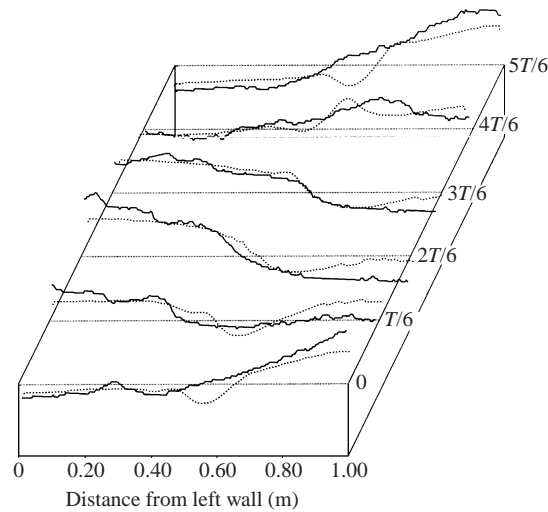
FIGURE 16. Simulated free-surface shape (Tank A): – – – – –, numerical simulation $U_0 = 0.50$ m s^{-1} and $H = 0.55$ m; ——, experiment $U_0 = 0.75$ m s^{-1} and $H = 0.55$ m.

amplification of the free-surface fluctuation caused by the initial inlet flow. That is to say, the reverse flow pattern could not be observed in the simulation.

3.2.2. *Numerical self-induced sloshing*

Figures 15(a) and 15(b) show examples of simulated free-surface oscillation. The amplitude of the free-surface fluctuation increased and decreased according to simulation conditions (U_0, H). This indicates the occurrence of 'numerical self-induced sloshing' as shown in figure 15(a) and the damping of sloshing motion the 'stable condition' as shown in figure 15(b).

Figure 16 shows the simulated and experimental deformation of free-surface shape over an oscillation period. The simulated free-surface shape is consistent with first mode sloshing. The nonlinear surface wave was similarly observed in simulation results, and propagated periodically against free-surface flow. The amplitude of numerical self-induced sloshing was about a third of that in the experiment. This quantitative discrepancy is attributed to the simulation assumption of high viscosity coefficient. However, the simulated water level variation and free-surface shape agree qualitatively with the experiment.
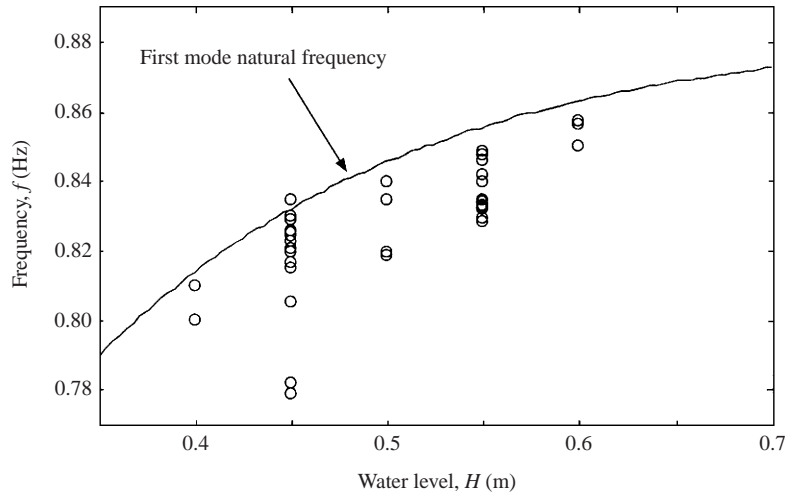
FIGURE 17. Frequency of numerical self-induced sloshing.

3.2.3. *Simulated oscillation frequency*

Figure 17 shows the relationship between simulated frequencies and water level H. The curve represents the theoretical eigenvalue in a two-dimensional tank from (2.1). Simulated frequencies were almost equal to theoretical frequencies, and were consistent with the experimental results.

3.2.4. *Simulated excitation map*

Figure 18 shows the simulated excitation map with respect to inlet velocity U_0 and inlet–surface distance $h = H - B$, where the experimental sloshing condition is also shown for comparison. In the simulation, the sloshing condition ($\bigcirc$) was distributed in the lower velocity and lower water level region. The stable state ($\times$) was observed with increasing inlet velocity or water level. The sloshing condition was restricted with respect to U_0 and h. These findings are similar to the experimental results. The simulation diverged in the high velocity condition ($\triangle$) because of the turbulent free surface.

Furthermore, numerical self-induced sloshing was observed under two separate conditions: high velocity *sloshing A* and low velocity *sloshing B*. The free-surface oscillation could not be self-excited between these sloshing conditions, where the stable condition prevailed. These two sloshing conditions were found to correspond qualitatively to first and second stage sloshing in the experiment, respectively.

The simulated sloshing velocity conditions were about $0.1\,\mathrm{m\,s}^{-1}$ lower than experimental conditions. This discrepancy is considered to be caused by the difference in Reynolds number (viscous rate) and the two-dimensional laminar simulation.

Several experimental characteristics of sloshing condition were identified in the simulation results. In particular, the two separate sloshing conditions are very similar to those in the experiment. Nevertheless, the physical correspondence of the respective sloshing conditions should be examined in detail. Therefore, the relationship between inlet velocity U_0 and other characteristics such as growth ratio, frequency and the jet streak line was examined in a similar way to the experiment.
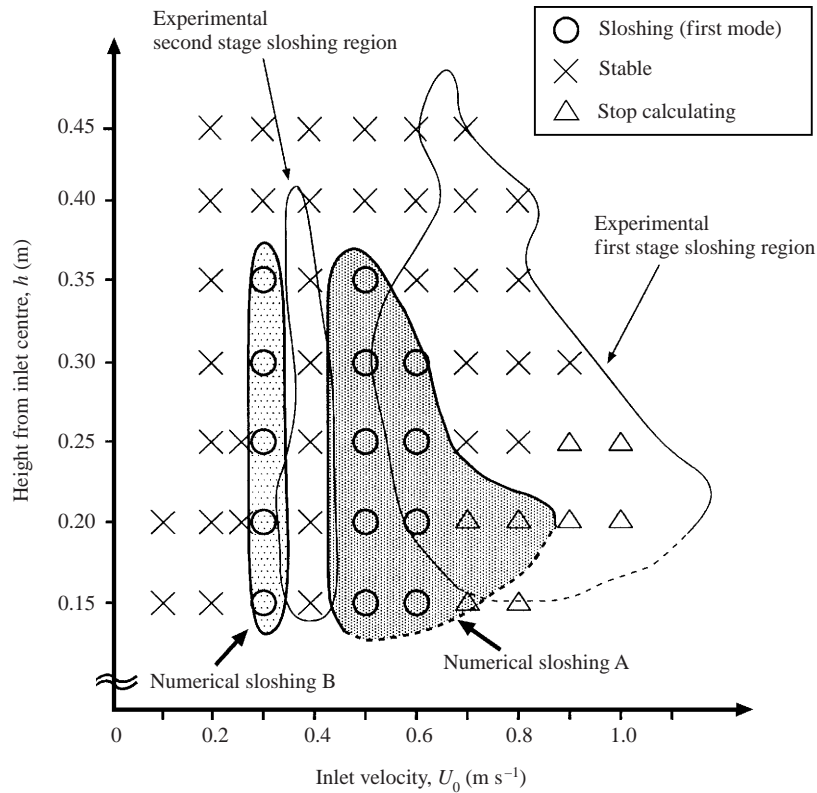
FIGURE 18. Simulated excitation map (Tank A).

3.2.5. *Simulated growth ratio*

As shown in figure 19, the normalized growth rate G was calculated from the simulated surface variation. The occurrence of numerical self-induced sloshing can be determined quantitatively by the value of G. With increasing inlet velocity, G tended to decrease rapidly, resulting in the stable condition ($G < 0$). With increasing water level, G also tended to shift toward negative values. These tendencies agree well with those of the experiment, as shown in figure 9.

As evident from figure 19, numerical self-induced sloshing occurs under two separate conditions. Under the lower inlet velocity condition ($U_0 \approx 0.3\,\mathrm{m\,s^{-1}}$, sloshing B), and the higher inlet velocity condition ($U_0 \approx 0.6\,\mathrm{m\,s^{-1}}$, sloshing A), the simulated growth ratio G is positive. G exhibits a negative peak between sloshing A and sloshing B conditions ($U_0 \approx 0.4\,\mathrm{m\,s^{-1}}$), and the stable condition prevails. In the experiment, there was a similar negative peak at $U_0 \approx 0.5\,\mathrm{m\,s^{-1}}$, as shown in figure 9. Therefore, the experimental characteristics of growth ratio G are represented accurately by the numerical simulation.

3.2.6. *Relationship between simulated frequency and inlet velocity*

Simulated frequencies are plotted in figure 20 with respect to inlet velocity U_0. Sloshing frequencies in the simulation were observed to be lower than the natural frequency, and tended to increase for each water level condition with increasing inlet velocity U_0. As shown in figure 10, similar tendencies were observed in the experiment.
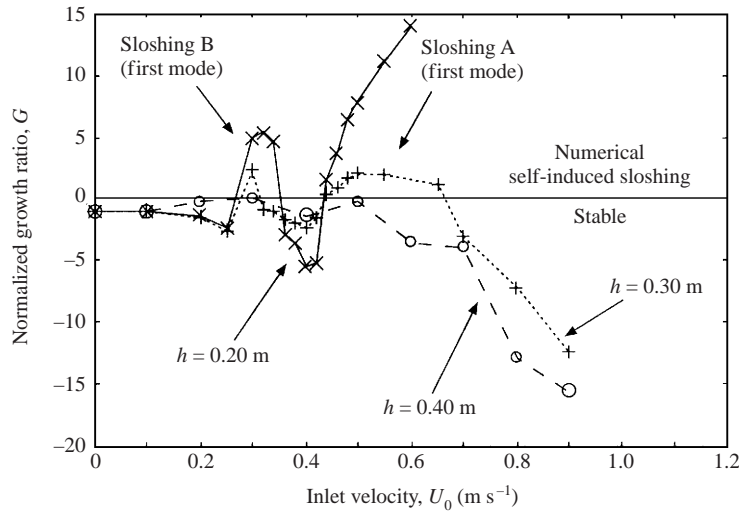
FIGURE 19. Relationship between U_0 and simulated growth ratio G.
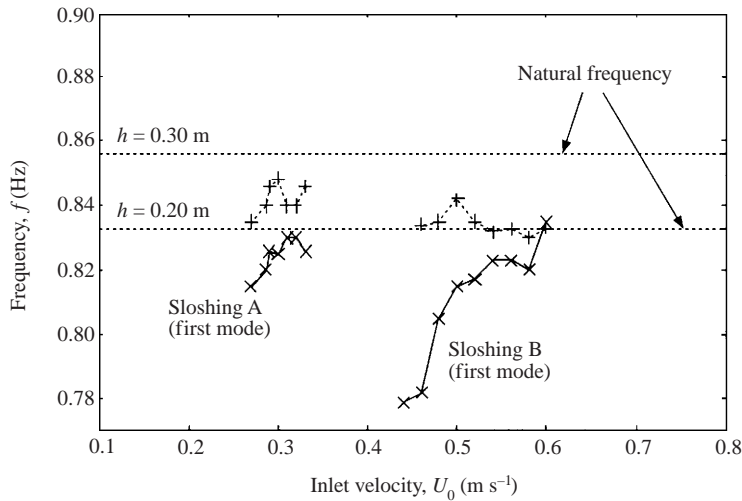
FIGURE 20. Relationship between U_0 and simulated frequency f.

Consequently, simulated frequencies indicate that numerical self-induced sloshing has the same excitation mechanism as in the experiment.

3.2.7. *Simulated jet streak line*

Figures 21(*a*) and 21(*b*) show simulated jet streak lines which are plotted at 1/4 sloshing period intervals under the two sloshing conditions of $U_0 = 0.5\,\mathrm{m\,s}^{-1}$ (sloshing A) and $U_0 = 0.3\,\mathrm{m\,s}^{-1}$ (sloshing B). It was observed that the jet streak lines fluctuated periodically and wavily with different modes. The jet fluctuation of sloshing B was found to be almost twice as wavy as that of sloshing A. These results are very similar to experimental observations of jet flow obtained by PIV, as shown in figure 11(*a*) and 11(*b*). Therefore, the separate conditions of numerical self-induced sloshing, A and B, are thought to correspond to the experimental first and second stage sloshing, respectively.
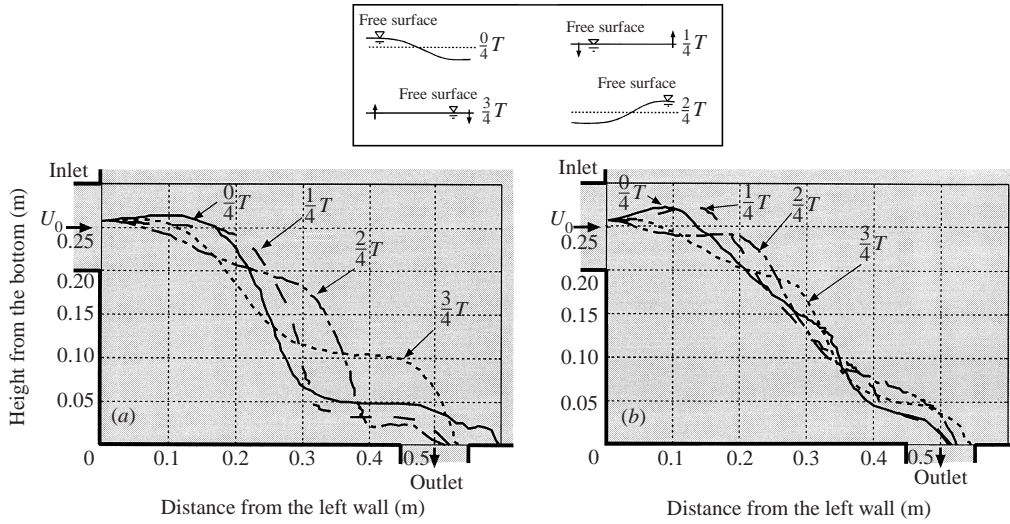
FIGURE 21. Simulated jet streak line: (*a*) sloshing A ($U_0 = 0.50\,\mathrm{m\,s^{-1}}$, $h = 0.20\,\mathrm{m}$), and (*b*) sloshing B ($U_0 = 0.30\,\mathrm{m\,s^{-1}}$, $h = 0.20\,\mathrm{m}$).

From a qualitative verification, the sloshing growth mechanism in the simulation is thought to be the same as that in the experiment. Therefore, the growth mechanism of self-induced sloshing can be investigated quantitatively using simulation results.

4. Analysis of growth mechanism

4.1. *Analysis method*

Self-induced oscillating phenomena have been explained using certain feedback processes such as *edge tone* (Blake 1986; Rockwell & Naudascher 1979). However, complex dynamics generally make it very difficult to determine the feedback process in full from an experimental or theoretical approach. The feedback process in self-induced sloshing is considered to be closed, on the basis of flow–surface interaction, which is actually composed of several complicated processes. In this study, the numerical simulation provides significant time-series and space-distribution data, which are highly effective in evaluating the feedback process. Therefore, the analysis of the feedback process was carried out to examine sloshing growth quantitatively using the simulation results.

Figure 22 shows the simplified feedback process proposed for use in the analysis of growth mechanism. The sloshing motion and the unsteady flow are considered separately to approximate simply the flow–surface interaction. Free-surface oscillation is defined as the sloshing motion based on potential analysis, while unsteady flow is given by numerical simulation. The effect of unsteady flow on sloshing motion was investigated as shown in figure 22; it is represented by the oscillation energy E_n supplied to the sloshing motion by the unsteady flow over a sloshing period.

The simulation results show that the flow field results entirely from the interaction between the sloshing motion and unsteady flow including the jet. The flow in the sloshing motion can not be directly separated from the unsteady flow. Therefore, free-surface oscillation is defined as the sloshing potential $\phi_s(x, y, t)$ by approximation of the free-surface shape. On the other hand, unsteady flow is represented as the fluctuation of force on a fluid volume F_n. The oscillation energy supplied for sloshing
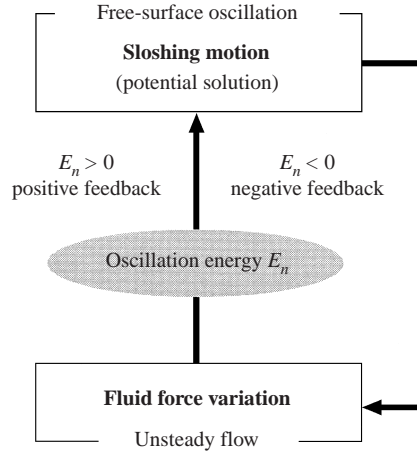
Free-surface oscillation

Sloshing motion
(potential solution)

$E_n > 0$
positive feedback

$E_n < 0$
negative feedback

Oscillation energy E_n

Fluid force variation
Unsteady flow

FIGURE 22. Growth mechanism analysis (feedback process).

E_n is calculated from $\phi_s(x, y, t)$ and $\boldsymbol{F}_n$ as explained in the following section. E_n and the distribution of oscillation energy $\overline{\Delta E_n}(x, y)$ can be calculated for the whole tank. In this study, the characteristics of E_n and $\overline{\Delta E_n}(x, y)$ are analysed. A growth mechanism for self-induced sloshing is quantitatively investigated by means of the feedback analysis.

4.2. *Calculation of oscillation energy supplied for sloshing*

4.2.1. *Sloshing potential*

Natural sloshing motion dominates self-induced sloshing, as shown in figures 7 and 17. Natural sloshing can be expressed in terms of the potential flow. The first mode sloshing potential is given by (Lamb 1932)

$$\phi_s(x, y, t) = a \frac{\omega_s W}{\pi} \frac{\cosh \pi(y + H)/W}{\sinh \pi H/W} \sin(\pi x/W) \sin(\omega_s t + \delta), \qquad (4.1)$$

where ω_s, W and H denote angular sloshing frequency, tank width and water level, respectively. The amplitude a and time phase δ are determined from the simulated surface shape with the least-squares technique.

4.2.2. *Forces on a fluid volume*

In this analysis, the force on a fluid volume $\boldsymbol{F}_{unst}$ caused by unsteady flow can be calculated by means of momentum theory, which is represented as the volume-integrated form of the Navier–Stokes equation:

$$\underbrace{\frac{\mathrm{d}}{\mathrm{d}t} \int_V \rho \boldsymbol{u} \, \mathrm{d}V}_{\boldsymbol{F}_{unst}} = \underbrace{\left(-\int_S \rho \boldsymbol{u}(\boldsymbol{u} \cdot \boldsymbol{n}) \, \mathrm{d}S\right)}_{\boldsymbol{F}_{con}} + \underbrace{\left(-\int_V (\mathrm{grad}\, p + \rho \boldsymbol{g}) \, \mathrm{d}V\right)}_{\boldsymbol{F}_{press}} + \underbrace{\int_V \rho \, v \nabla^2 \boldsymbol{u} \, \mathrm{d}V}_{\boldsymbol{F}_{diss}},$$

$$(4.2)$$

where S and V denote a surface and a volume in a control surface, respectively; $\boldsymbol{n}$ denotes a normal vector on a control surface. The present feedback analysis can be used to investigate the significance of the terms in the Navier–Stokes equation, $\boldsymbol{F}_{con}$, $\boldsymbol{F}_{press}$ and $\boldsymbol{F}_{diss}$. Therefore, each force $\boldsymbol{F}_n$ was separately calculated from the simulation results.

The fixed control volume should be defined as the calculation mesh in the calculation of the forces. In this simulation, however, the physical mesh of the BFC region is deformed because of the free-surface movement. Therefore, the velocity and pressure fluctuations in a fixed control volume were interpolated from the data in the BFC region.

4.2.3. *Oscillation energy*

The effect of forces on natural sloshing motion was evaluated quantitatively in terms of the oscillation energy supplied for sloshing E_n. Oscillation energies in a control volume for a unit time $\Delta E_n(x, y, t)$ can be calculated as an inner product between the forces $\boldsymbol{F_n}(x, y, t)$ and the sloshing velocity (grad $\phi_s(x, y, t)$) in a control volume:

$$\Delta E_n(x, y, t) = \boldsymbol{F_n}(x, y, t) \cdot \operatorname{grad} \phi_s(x, y, t), \tag{4.3}$$

where subscript n denotes terms in the Navier–Stokes equation, i.e. *con*, *press*, *diss* and *unst*. The local oscillation energy $\overline{\Delta E_n}(x, y)$ over a natural sloshing period T_s can be expressed by

$$\overline{\Delta E_n}(x, y) = \oint_{T_s} \Delta E_n(x, y, t) \, dt. \tag{4.4}$$

It is space-integrated for the whole field, so the oscillation energy E_n supplied for the sloshing motion can expressed as

$$E_n = \frac{1}{WHa^2} \int_{S_{tank}} \overline{\Delta E_n}(x, y) \, dS, \tag{4.5}$$

where S_{tank} denotes the two-dimensional area of the tank. Oscillation energy is converted into energy per unit mass $WH = S_{tank}$ and the square of the amplitude a^2.

Oscillation energy for the unsteady term E_{unst} is theoretically equivalent to the sum of the other oscillation energies. However, a numerical error δe was introduced to compensate for errors in the calculation. The sources of this error are considered to be the staggered mesh used in the numerical simulation, and the interpolation of velocity and pressure in the BFC region. E_{unst} is considered to be equal to the sum of the other oscillation energies and δe,

$$E_{unst} = E_{con} + E_{press} + E_{diss} + \delta e. \tag{4.6}$$
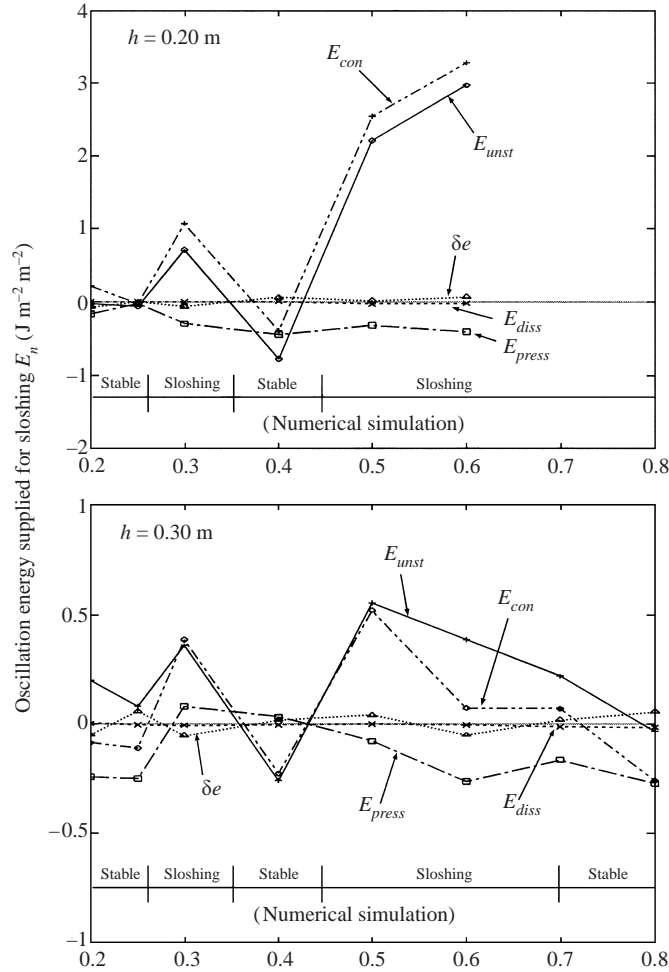
4.3. *Results of growth mechanism analysis*

Oscillation energies E_n were obtained from the simulation results under certain conditions of inlet velocity U_0 and inlet–surface distance h. Figure 23 shows E_n and numerical error δe with respect to U_0. For all conditions, δe was estimated to be less than 10% of the maximum absolute value of E_n. Therefore, the balance of energy is well represented in the calculation of oscillation energy, and E_n can be utilized for quantitative evaluation.

4.3.1. *Oscillation energy supplied for sloshing*

Unsteady term: E_{unst}   Figure 24 shows E_{unst} and normalized growth ratio G with respect to inlet velocity U_0. When E_{unst} is positive ($E_{unst} > 0$), self-induced sloshing is excited ($G > 0$). When E_{unst} is negative ($E_{unst} < 0$), the sloshing motion is damped ($G < 0$). Additionally, the tendency for E_{unst} to become smaller with increasing water level is very similar to that of the growth ratio G.

As E_{unst} is the total sum of oscillation energy E_n, as shown by (4.6) and the sign

FIGURE 23. Oscillation energy supplied for sloshing E_n.

and magnitude of E_{unst} was found to be related to the growth ratio G, this confirms the validity of this growth mechanism analysis.

The other terms: E_{con}, E_{press}, E_{diss}   As is evident from figure 23, the sign of oscillation energy for the convection term E_{con} corresponds to sloshing growth like E_{unst}. When E_{con} is positive ($E_{con} > 0$), self-induced sloshing is excited. This analytical result shows that E_{con} can be used to quantitatively predict the occurrence of self-induced sloshing. As the pressure term E_{press} appears to be independent of sloshing, and the dissipation term E_{diss} is much lower than any other oscillation energy they are considered to have no effect on sloshing growth at all.

Among the other terms, the convection term E_{con} was found to contribute most to sloshing growth. Therefore, it was quantitatively determined that sloshing motion was self-excited by the nonlinear force caused by flow variation.

4.3.2. *Oscillation energy distribution*

In order to examine the growth mechanism in detail, the oscillation energy distribution $\overline{\Delta E_n}(x, y)$ was calculated, as it can convey the spatial characteristics of the
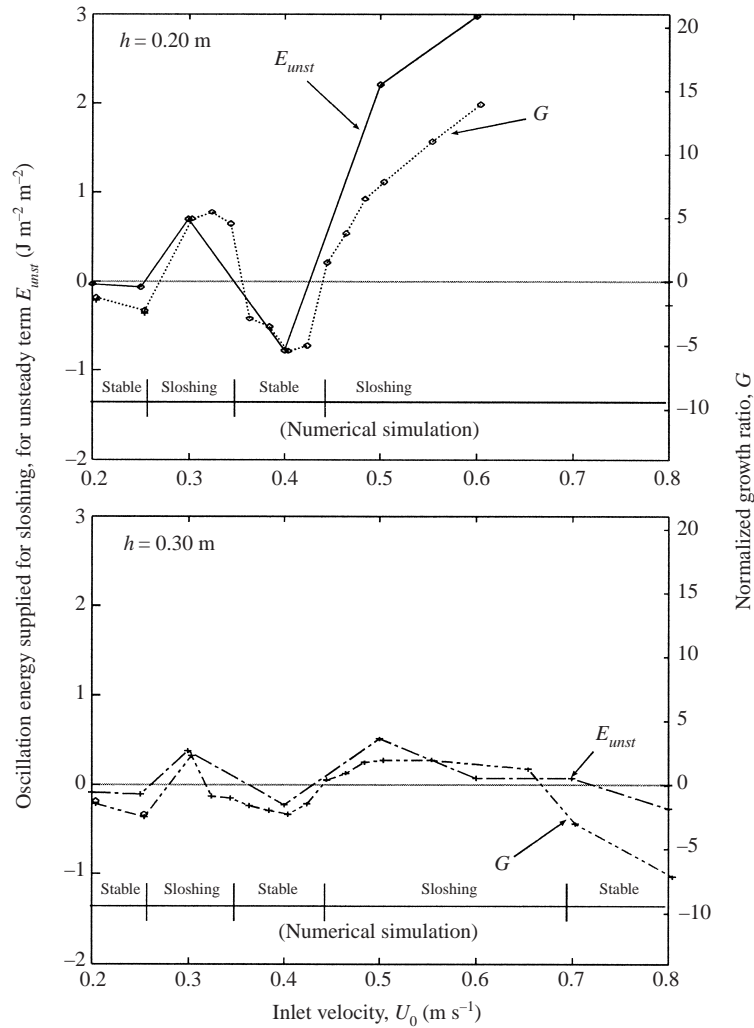
FIGURE 24. Comparison between E_{unst} and growth ratio G.

interaction between unsteady flow and sloshing motion. As described above, E_{con} turns out to govern the sloshing growth. The oscillation energy distribution for the convection term $\overline{\Delta E_{con}}(x, y)$ is explained as follows.

The convection term: $\overline{\Delta E_{con}}(x, y)$ Figure 25(*a–f*) shows $\overline{\Delta E_{con}}(x, y)$ under the conditions of $U_0 = 0.20 \sim 0.70 \, \mathrm{m \, s^{-1}}$ and $h = 0.30 \, \mathrm{m}$. For all conditions, the absolute value of local oscillation energy is observed to be greatest along the jet. The alternating-sign energy patterns are exhibited along the flow path from inlet to outlet. The number of inversions of local oscillation energy decreases with increasing inlet velocity U_0. This suggests that sloshing growth is determined by jet fluctuation and inlet velocity U_0. The arrangement of the oscillation energy pattern, which was related to the spatial phase state of jet fluctuation, was examined in respect to U_0.

In figure 25(*c*), the local oscillation energy pattern is $- + - +$ between inlet and outlet. Table 2 shows the arrangement of the local oscillation energy patterns along the jet. With increasing U_0, this varies in the sequence $- + - + - +, - + - + -,$ $- + - +, - + - , - +, -$. When the arrangement is $- + - + -, - + -$ or $-$, self-
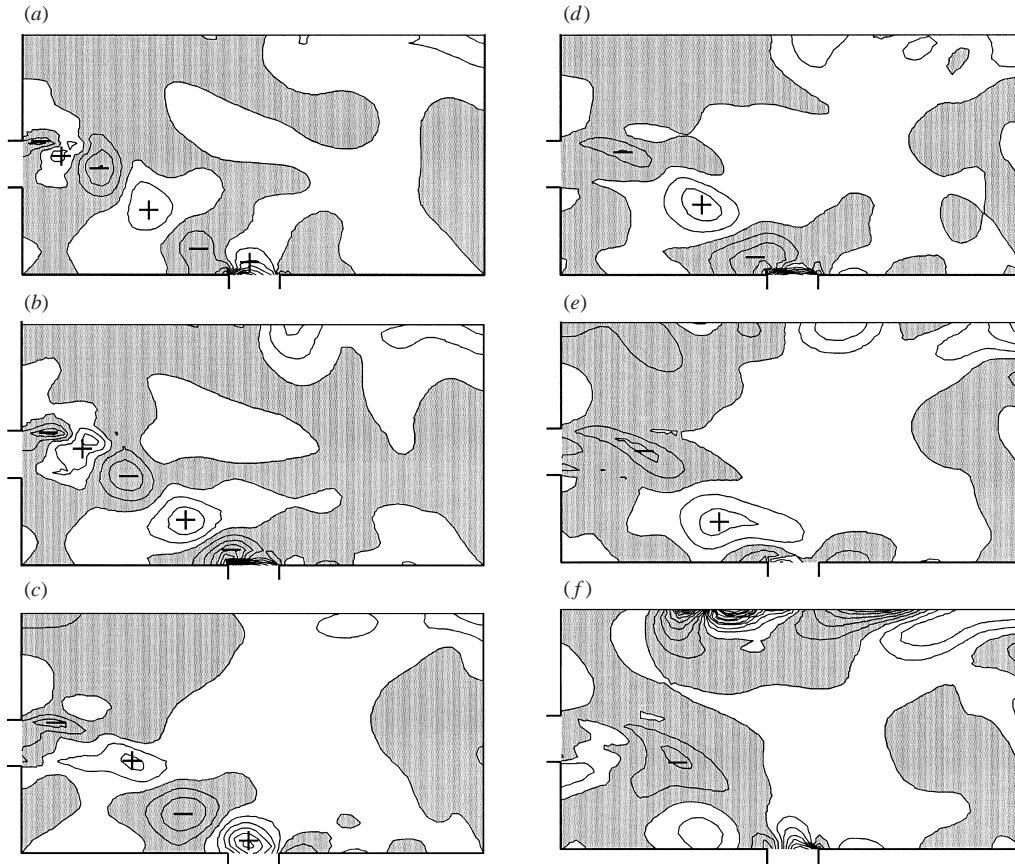
FIGURE 25. (*a–f*) Oscillation energy distribution for convection term $\Delta E_{con}(x, y)$ under the condition of $h = 0.30\,\mathrm{m}$): (*a*) $U_0 = 0.20\,\mathrm{m\,s^{-1}}$ stable condition ($\times$), (*b*) $U_0 = 0.25\,\mathrm{m\,s^{-1}}$ stable condition ($\times$), (*c*) $U_0 = 0.30\,\mathrm{m\,s^{-1}}$ sloshing B condition ($\bigcirc$ B), (*d*) $U_0 = 0.40\,\mathrm{m\,s^{-1}}$ stable condition ($\times$), (*e*) $U_0 = 0.50\,\mathrm{m\,s^{-1}}$ sloshing A condition ($\bigcirc$ A), (*f*) $U_0 = 0.80\,\mathrm{m\,s^{-1}}$ stable condition ($\times$).

Sloshing status	($U_0\,\mathrm{m\,s^{-1}}$, $h\,\mathrm{m}$)	Arrangement of $\overline{\Delta E_{con}}(x, y)$ along jet
$\times$	(0.20, **0.20**)	$- + - + - +$
$\times$	(0.25, 0.20)	$- + - + -$
$\bigcirc$A	(0.30, 0.20)	$- + - +$
$\times$	(0.40, 0.20)	$- + -$
$\bigcirc$B	(0.50, 0.20)	$- +$
$\bigcirc$B	(0.60, 0.20)	$- +$
$\times$	(0.20, **0.30**)	$- + - + - +$
$\times$	(0.25, 0.30)	$- + - + -$
$\bigcirc$A	(0.30, 0.30)	$- + - +$
$\times$	(0.40, 0.30)	$- + -$
$\bigcirc$B	(0.50, 0.30)	$- +$
$\bigcirc$B	(0.60, 0.30)	$- +$
$\times$	(0.70, 0.30)	$-$
$\times$	(0.80, 0.30)	$-$

TABLE 2. Arrangement of oscillation energy pattern along jet for convection term.

induced sloshing cannot occur at all. When the number of positive local oscillation energy peaks is less than that of negative peaks along the jet, sloshing motion is damped. Under two inlet conditions of $U_0 = 0.50$–0.60 and $U_0 = 0.30\,\mathrm{m\,s^{-1}}$, the number of positive local oscillation energy peaks is equal to that of negative peaks, $- + - +$ and $- +$. Hence, self-induced sloshing is considered to occur in these two separate regions as sloshing A and sloshing B, respectively.

For $U_0 = 0.20\,\mathrm{m\,s^{-1}}$, the number of positive local oscillation energy peaks $- + - +$ $- +$ is equal to that of negative peaks. However the growth rate G was exceptionally negative and the sloshing motion was damped, as shown in figure 24. It is thought that the inlet energy at this low velocity $U_0 = 0.20\,\mathrm{m\,s^{-1}}$ is insufficient for E_{con} to sustain self-induced sloshing.

From this qualitative evaluation, it has been clarified that the growth mechanism of self-induced sloshing is dependent on the arrangement of the oscillation energy pattern along the jet. In contrast, circulating flow and under-surface flow are considered not to be significant in the growth mechanism. Consequently, unsteady jet flow is thought to supply the sustaining energy for the sloshing motion. It was concluded that its spatial phase state determined whether or not jet fluctuation could cause the sloshing motion to be self-excited.

5. Discussion

5.1. *Governing parameter*

From the analysis of the growth mechanism, the excitation of self-induced sloshing was considered to be dependent on the spatial phase state of jet fluctuation. Jet fluctuation resulted in the wave travelling from inlet to outlet, i.e. emerging large vortices, as shown in figure 11.

It is well known that a jet is intrinsically unstable. Jet behaviour can be explained generally using the Strouhal number $St = f_r l_r / U_r$, where f_r, l_r and U_r denote the representative frequency, length and velocity, respectively. In the present study, a modified Strouhal number St_s is proposed to evaluate the spatial characteristics of jet fluctuation under sloshing conditions. St_s is derived from the general Strouhal number St in the following.

The frequency of natural sloshing f_s^n in (2.1) provides f_r in St, because jet fluctuation is synchronized with the sloshing motion. The experimental results indicated that the location of inlet B and outlet S, which determined tank geometry, had a significant effect on the excitation of self-induced sloshing. Therefore, the representative length l_r in St must be defined according to the tank geometry. In this derivation, the distance between inlet and outlet $L = \sqrt{B^2 + S^2}$ is substituted for l_r. U_r in St is assumed to be the dominant phase velocity u_{con} of turbulent jet disturbances caused by instability of the shear layer, because u_{con} is thought to determine jet fluctuation. Turbulent shear flow is generally unstable, resulting in the generation of disturbances. Disturbances are transported by unsteady and non-uniform jet flow. Hence, the disturbances have different phase velocities, but have a certain dominant phase velocity u_{con} in their interaction. The velocity gradient of the jet is largest at the position where jet velocity is approximately half of the jet centreline velocity u_m. Blake (1986) suggested that u_{con} was approximately equal to $u_m/2$, which was the velocity at the most unstable position:

$$u_{con} \approx \tfrac{1}{2} u_m(x). \tag{5.1}$$

Taking account of the spatial damping of a turbulent jet disturbance, the jet

centreline velocity u_m can be defined as a function of the propagation direction x of the jet. The application of (5.1) to the appropriate parameters in St results in the modified Strouhal number St_s:

$$St_s = f_s^n \int_0^L \frac{dx}{u_{con}} \approx f_s^n \int_0^L \frac{dx}{u_m(x)/2}. \tag{5.2}$$

As seen from (5.2), St_s represents the time, as a multiple of a sloshing period, for the turbulent jet disturbance to propagate distance L between inlet and outlet. Therefore, St_s indicates the wavenumber of the turbulent jet disturbance, i.e. the number of large vortices that occur from inlet to outlet over a sloshing period.

The integration in (5.2) was calculated using the experimental velocity distribution of the turbulent free jet. Abramovich (1963) reported the experimental damping of the jet centreline velocity u_m as

$$u_m(x) = \frac{1.2U_0}{\sqrt{\alpha(x + 0.41b)/b}}, \tag{5.3}$$

where b is inlet width and $\alpha \approx 0.22$ is an experimental constant. The origin is set at the centre of the inlet; the x- and y- axes are in the horizontal and vertical directions, respectively. However, (5.3) fails to consider effects of tank walls, free surface and circulating flow, etc. on the jet. The potential core of the jet cannot be calculated precisely using this equation, because jet flow was observed to curve from inlet to outlet. In the present derivation, therefore, these effects were assumed to be negligible so that the jet–flow system could be simplified, and then (5.3) was only used tentatively. Substituting (5.3) into (5.2), St_s can be expressed with the approximation $L \gg b$ as follows:

$$St_s = \frac{f_s^n L}{U_0} \kappa \sqrt{\frac{L + 2b}{b}}, \tag{5.4}$$

where $\kappa \approx 0.67$ is an experimental constant and $\sqrt{(L + 2b)/b}$ represents the effect of the tank geometry.

Equation (5.4) was applied to the experimental results and then each value of St_s was plotted for all tank geometry cases (Okamoto & Madarame 1991; Okamoto 1993; Fukaya *et al.* 1995). Figure 26 shows the excitation maps for each tank, with respect to St_s and inlet–surface distance divided by tank width h/W. As evident from figure 26, the excitation of self-induced sloshing is characterized well using St_s across all tank geometries and sloshing modes. In all cases, self-induced sloshing is observed to occur only when the modified Strouhal number is $St_s \approx 1.0$ or ≈ 2.0. The two sloshing conditions are separated and fall within an excitation band proximal to a discrete integer number of 1 or 2. The conditional equation of the excitation of self-induced sloshing is proposed:

$$m - 0.25 < St_s < m + 0.25 \quad (m = 1 \text{ or } 2\ldots), \tag{5.5}$$

where m denotes a discrete integer number, and indicates the approximate number of large vortices that emerge from inlet to outlet by sloshing motion. The excitation band represents a quarter-phase of jet oscillation $\pm\pi/4$ and is defined as $m \pm 0.25$ around St_s of 1 or 2. The sloshing stage is determined from $m = 1$ for first stage sloshing or $m = 2$ for second stage sloshing. Therefore, when the wavenumber of the wavy jet, i.e. the number of large vortices emerging along the inlet–outlet flow, is satisfied by (5.5), either first or second stage self-induced sloshing is excited.

From the images of jet fluctuation in figure 11, the wavenumber of jet fluctuation
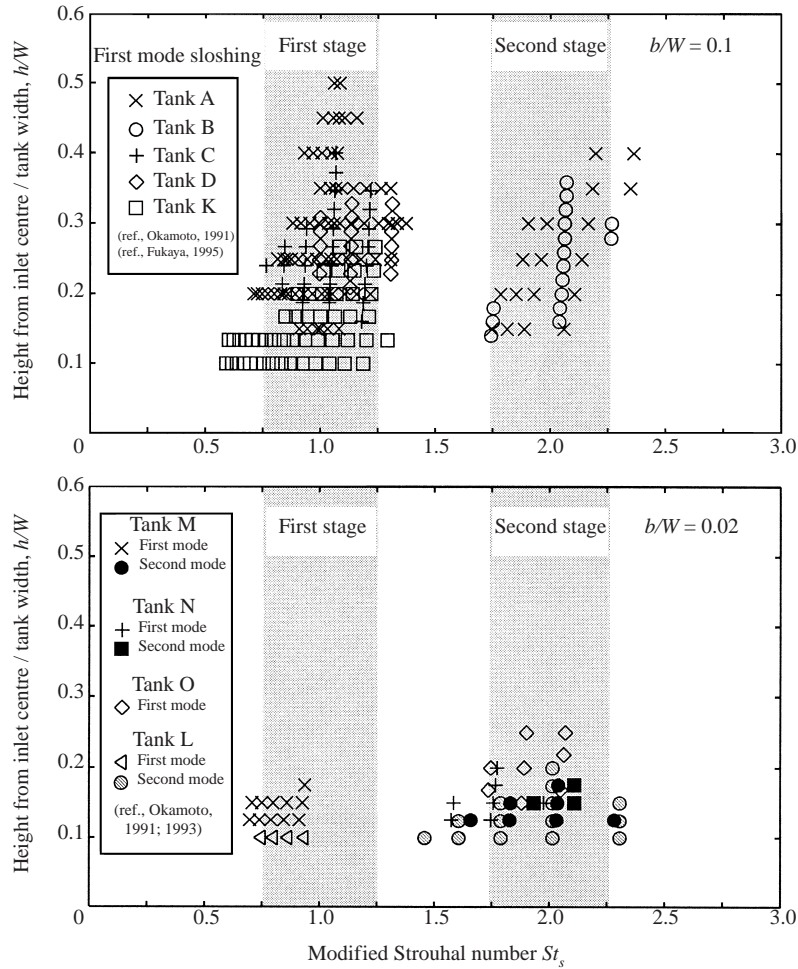
FIGURE 26. Modified Strouhal number St_s.

was demonstrated to be about 1 for first stage sloshing or 2 for second stage sloshing. The sloshing conditions predicted by St_s were validated experimentally.

The modified Strouhal number St_s has been found to be a governing parameter of self-induced sloshing excited by a horizontally injected plane jet. It was experimentally confirmed that the spatial phase state of jet fluctuation determined the sloshing excitation, which was similar to the results of growth mechanism analysis.

5.2. *Sloshing mode shift and jet stage transition*

In Tanks A, M and N, either the sloshing mode or jet stage was observed to change, as shown in figures 8(*a*), 8(*c*), 8(*d*) and 26. It is thought that the excitation mechanism of self-induced sloshing is related to a sloshing mode shift and a jet mode (stage) transition, which are caused by variations of inlet velocity U_0. The excitation map with respect to Reynolds number Re and St_s was examined in order to clarify the dependence of sloshing on U_0. St_s indicates the jet mode (stage) m, so the shift in sloshing mode n and the transition of jet stage m can be evaluated from this map.

Figures 27(*a*)–27(*c*) show the relevant excitation maps for Tanks A, M and N, respectively. The two shaded regions represent the excitation requirements from (5.5).
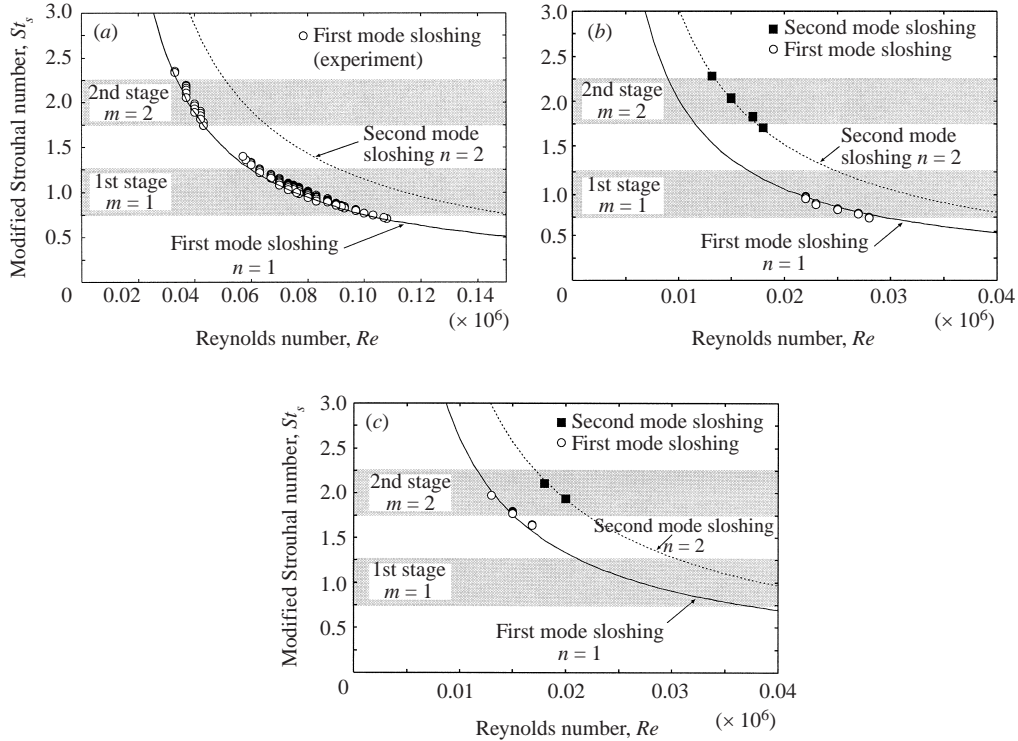
FIGURE 27. The relation between Re and St_s: (*a*) Tank A, (*b*) Tank M, (*c*) Tank N.

When the frequency is fixed at a natural sloshing eigenvalue f_s^n, the relation between Re and St_s is hyperbolic $St_s \propto Re^{-1}$. The natural frequency f_s^n is a function of water level H. In this study, however, f_s^n varies by less than 4% with respect to H, because the regions of water levels for sloshing conditions are very narrow and relatively high. Therefore, f_s^n for each tank was calculated using the average value of all water level conditions. The two lines in each figure represent $St_s \propto Re^{-1}$ as applied to the sloshing frequencies of the first and second modes corresponding to $n = 1$ and $n = 2$, respectively. Self-induced sloshing is excited at the intersection of the hyperbola and shaded regions, because sloshing conditions must be satisfied by (5.5). Self-induced sloshing was proven to occur at these intersection conditions in all tank geometry cases.

As shown in figure 27(*a*), the jet stage transition in Tank A occurs from $m = 2$ to $m = 1$ for the same first mode sloshing ($n = 1$), with increasing inlet velocity U_0. On the other hand, figure 27(*c*) shows that the sloshing mode in Tank N shifts from $n = 1$ to $n = 2$ in the same second jet stage ($m = 2$). Figure 27(*b*) shows that, in Tank M, the second mode sloshing in the second stage ($n = 2, m = 2$) changes to the first mode sloshing in the first stage ($n = 1$, $m = 1$).

The combination (n, m) of sloshing mode and jet stage was found to change according to tank geometry and U_0. The state of self-induced sloshing can be determined from this combination (n, m), and it is successfully predicted that two sloshing conditions at the same mode or multi-mode sloshing can occur at different and separate conditions of U_0. In particular, this explains well how the multi-mode sloshing conditions can have opposite distributions with U_0, as shown in figures 8(*c*) and 8(*d*). The intersection conditions in figure 27 predict that further self-induced sloshing could
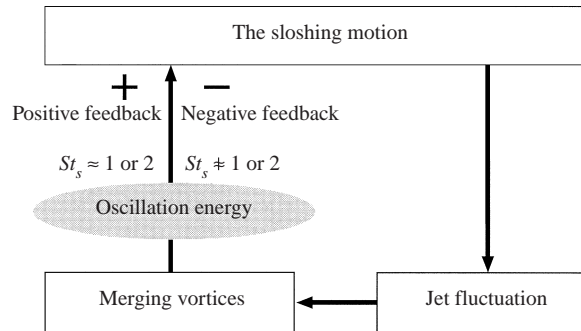
FIGURE 28. Excitation mechanism of self-induced sloshing.

occur at conditions where sloshing cannot be observed experimentally. However, it is thought that these predicted self-induced sloshings cannot be excited because of too low an inlet velocity, too high a flow velocity below the free surface and the clustering of sloshing conditions as seen experimentally.

5.3. *Feedback mechanism*

In §4, a simplified feedback process was proposed for the analysis of the growth mechanism, as shown in figure 22. This model was validated using the simulation results. Jet fluctuation played an important role in sloshing growth, in that it supplied the sustaining-energy for the sloshing motion. A governing parameter St_s was derived, which described sloshing behaviour using experimental results. It was confirmed that the phase state of jet fluctuation was a significant factor in the excitation mechanism of self-induced sloshing. As a result of these evaluations, based on the simplified feedback model in figure 22, it is possible to propose a new excitation mechanism of self-induced sloshing.

Figure 28 shows a schematic diagram of the proposed excitation mechanism. The jet is fluctuated by a pressure oscillation that is synchronized with sloshing motion. The jet fluctuation generates one or two large vortices that emerge from inlet to outlet, the number of which is dependent on inlet velocity U_0 and tank geometry of inlet–outlet distance L and inlet width b. The positive feedback energy ($E_{con} > 0$) for the sloshing motion is supplied by jet fluctuation itself when the number of emerging large vortices is satisfied by (5.5). In such conditions, the positive feedback loop in figure 28 is closed and the sloshing motion can grow. This feedback mechanism is thought to clarify the excitation of self-induced sloshing.

It is well known that the 'edge tone' is explained using a feedback loop composed of the interaction between jet fluctuation and pressure variation (Rockwell & Naudascher 1979; Blake 1986). This is similar to our proposed excitation mechanism of self-induced sloshing. Moreover, the edge tone phenomenon has similar characteristics to self-induced sloshing, such as the governing parameter St_e and the conditional equation. St_e is defined as $St_e = f_e L_e / u_{con}$, where f_e and L_e denote the edge tone frequency and inlet–edge distance, respectively. The conditional equation was experimentally found to be $St_e = m + 0.25$ (Rockwell & Naudascher 1979; Blake 1986).

However, the two phenomena are not considered to be entirely equivalent. Edge tone is thought to result from interaction between jet fluctuation and pressure variation caused by periodical impingement of the jet on the edge (Rockwell & Naudascher 1979; Blake 1986). Therefore, according to the conditional equation of St_e, the edge

tone frequency f_e is dependent on u_{con} and L_e, which are determined uniquely by the initial jet–edge system. When edge tone is generated, a phase lock between the inlet and edge must be established at f_e. The number of vortices m emerging between the inlet and edge over an oscillation period must be integral ($m = 1, 2, \ldots$).

On the other hand, self-induced sloshing is caused by the interaction between the different fluid motions of jet fluctuation and sloshing motion. Pressure oscillation is naturally induced by a free-surface oscillation, the frequency of which is locked by the sloshing motion. The representative length L in St_s varies according to changes in the average flow pattern, even if tank geometry is fixed. Hence, it is considered that a precise phase lock between inlet and outlet does not have to be established. Self-induced sloshing is excited when St_s is in an excitation band around a discrete integer number, as shown in (5.5).

Self-induced sloshing can be considered to be an edge tone with a resonator (Brackenridge & Nyborg 1956), because the frequency is fixed by a sloshing mode. Additionally, the frequency of self-induced sloshing tends to increase with inlet velocity U_0, as shown in figure 10. This tendency is similarly observed for the edge tone with a resonator. However, the sloshing motion is considered not only to fix the oscillation frequency, but also to act as another fluid motion that interacts with jet fluctuation. Thus, sloshing motion forms a part of the feedback mechanism, as shown in figure 28. The temporal and spatial interaction between the two fluid motions of jet fluctuation and sloshing motion is considered to affect the excitation of self-induced sloshing in the limited flow region of a tank. Hence, from these considerations, the excitation mechanism of self-induced sloshing is thought to be not entirely the same as that of the edge tone.

6. Conclusions

A self-induced free-surface oscillation, self-induced sloshing, was observed in a rectangular tank with a submerged and horizontally injected water jet, and its physical behaviour was evaluated experimentally. Self-induced sloshing was excited by the flow itself without any external force. The oscillation was dominant at about the first or second eigenvalue of the fluid in a tank. Sloshing conditions were found to be strongly dependent on inlet velocity and tank geometry.

A numerical code was developed to simulate self-induced sloshing. The simulation results were qualitatively verified by the experimental results, showing good agreement. Sloshing growth was analysed quantitatively in terms of the oscillation energy fed back to the sloshing motion E_{con}, which was calculated from simulation results. Self-induced sloshing was considered to be sustained by the feedback oscillation energy that was generated by the nonlinear interaction between sloshing motion and jet fluctuation. It was clarified that sloshing growth was primarily dependent on the spatial phase state of jet fluctuation. Circulating flow and free-surface flow were considered to be less significant to the excitation mechanism.

A governing parameter, the modified Strouhal number St_s, was derived. It was found that self-induced sloshing corresponded well in all experimental cases to St_s values of 1.0 (first stage) and 2.0 (second stage). A conditional equation (5.5) for the excitation of self-induced sloshing was proposed. St_s was demonstrated to be a dimensionless parameter that indicated the wavenumber of the wavy jet, i.e. the number of large vortices which emerge between inlet and outlet through sloshing motion. It was proven that St_s was a governing parameter of this phenomenon. Using St_s, the variations of U_0 were found to cause a sloshing mode n shift or a jet mode

(stage) m transition. The state of self-induced sloshing was identified and predicted by the combination of sloshing mode and jet stage (n, m). It has been clarified that certain sloshing conditions in the same mode, or multi-mode sloshing, can distribute differently over a single U_0 value.

We have proposed a new excitation mechanism of self-induced sloshing, which is represented by a simple feedback loop focusing on jet–surface interaction. Hence, the overall physical oscillation mechanism of self-induced sloshing has been clarified.

REFERENCES

ABRAMOVICH, G. N. 1963 *The Theory of Turbulent Jets*, p. 75. MIT Press.

ABRAMSON, H. N., CHU, W. H. & KANA, D. D. 1966 Some studies of nonlinear lateral sloshing in rigid containers. *Trans. ASME: J. Appl. Mech.* **88**, 777–784.

ADRIAN, R. J. 1991 Particle-imaging techniques for experimental fluid mechanics. *Ann. Rev. Fluid Mech.* **23**, 261–304.

AMANO, K. & IWANO, R. 1991 Experimental and analysis of jet-induced sloshing in a tank. *Trans. JSME (in Japanese)* B **57**, 1947–1954.

BRACKENRIDGE, J. B. & NYBORG, W. L. 1957 Acoustical characteristics of oscillating jet-edge systems in water. *J. Acoust. Soc. Am.* **29**, 459–463.

BLAKE, W. K. 1986 *Mechanics of Flow-Induced Sound and Vibration*, p. 130. Academic.

FUKAYA, M., BABA, M., OKAMOTO, K. & MADARAME, H. 1995 Self-induced sloshing caused by a jet from a rectangular tank wall. *Proc. HYDRA-2000, 26th, Congr. IAHR*, Vol. 1, pp. 468–473.

FUKAYA, M., OKAMOTO, K., MADARAME, H. & IIDA, M. 1993 Effects of tank geometries on self-induced sloshing caused by an upward plane jet. *Proc. JSME FIVES A-PVC*, Vol. 1, pp. 271–276.

HARA, F. 1990 Experimental study on sloshing characteristics of a flowing liquid in a tank. *JSME Intl J.* III **33**, 330.

INAGAKI, T., UMEOKA, T., FUJITA, K., NAKAMURA, T., SHIRAISHI, T., KIYOKAWA, T. & SUGIYAMA, Y. 1987 Flow induced vibration of inverted U-shaped piping containing flowing fluid of top entry system for LMFBR. *Trans. Intl Conf. on Structural Mechanics in Reactor Technology, Lausanne, 1987* (ed. F. H. Wittman), Vol. 9-E, pp. 295–302. Balkema.

KAWAHARA, T. & KUWAHARA, K. 1984 Computation of high Reynolds number flow around a circular cylinder with surface roughness. *AIAA Paper* 84-0340.

LAMB, H. 1932 *Hydrodynamics*, pp. 363–366. Cambridge University Press.

MADARAME, H., IIDA, M., OKAMOTO, K. & FUKAYA, M. 1993 Jet-flutter: self-induced oscillation of an upward plane jet impinging on a free surface. *Proc. JSME FIVES A-PVC*, Vol. 1, pp. 265–270.

MADARAME, H., OKAMOTO, K. & HAGIWARA, T. 1992 Self-induced sloshing in a tank with circulating flow. *Proc. ASME PV&P*, Vol. 232, pp. 5–11.

NICHOLS, B., HIRT, C. & HOTCHKISS, R. 1980 SOLA-VOF: A Solution Algorithm for Transient Fluid Flow with Multiple Free Surface. LA-8355.

OKAMOTO, K. & MADARAME, H. 1991 Self-induced oscillation of free surface in a tank with circulating flow. *Proc. 5th Intl Conf. on Flow Induced Vibrations* (ed. B. L. Clarkson), Vol. 6, pp. 539–545. IMechE.

OKAMOTO, K., FUKAYA, M. & MADARAME, H. 1993 Self-induced sloshing caused by flow in a tank. *ASME PV&P*, Vol. 258, pp. 105–111.

OKAMOTO, K., MADARAME, H. & HAGIWARA, H. 1992 Self-induced water level oscillation in a tank with flow Pattern transformation. *Proc. ASME PV&P*, Vol. 232, pp. 13–17.

ROCKWELL, D. & NAUDASCHE, K. 1979 Self-sustained oscillation of impinging free shear layers. *Ann. Rev. Fluid Mech.* **11**, 67–94.

TAKIZAWA, A. & KONDO, S. 1995 Computer discovery of the mechanism of flow-induced sloshing. *Proc. ASME PV&P*, Vol. 314, pp. 153–158.

TAKIZAWA, A., KOSHIZUKA, S. & KONDO, S. 1992 Generalization of physical component boundary fitted co-ordinate (PCBFC) method for the analysis of free surface flow. *Intl J. Numer. Meth. Fluids* **15**, 1213–1237.

TANAKA, N. & FUKUHARA, K. 1996 Numerical prediction of self-excited free surface sloshing. In *Flow Modeling Turbulence Measurements VI, Proc. 6th Intl Symp., Tallahassee, FL* (ed. Chen, Shih, Lienau & King), pp. 671–678. Balkema.